Universidade do Minho
Escola de Engenharia

Carlos Manuel Lima Oliveira

Control and readout electronics for miniaturized temperature sensors integrated with an organ-on-a-chip

Março de 2022

Control and readout electronics for miniaturized temperature sensors integrated with an organ-on-a-chip
Carlos Oliveira
UMinho | 2022

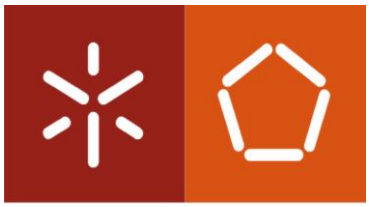

Universidade do Minho
Escola de Engenharia

Carlos Manuel Lima Oliveira

Control and readout electronics for miniaturized temperature sensors integrated with an organ-on-a-chip

Março de 2022

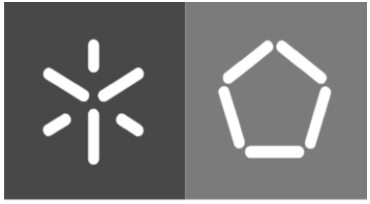

Universidade do Minho
Escola de Engenharia

Carlos Manuel Lima Oliveira

Control and readout electronics for miniaturized temperature sensors integrated with an organ-on-a-chip

Dissertação submetida na Universidade do Minho para obtenção do grau de
Mestre em Engenharia Eletrónica Industrial e de computadores

Trabalho efetuado sob a orientação do(s)
Professora Dr.ª Graça Minas e Dr.° Paulo Sousa

Março de 2022

ACKNOWLEDGEMENTS

I would like to thank Professor Graça Minas for the good orientation and opportunity to be a part of this project.

To Professor Paulo Sousa, a big thanks for all the guidance, knowledge, disponibility, and dedication to this orientation.

Also, thank Tiago Matos for all the support in the electronics and assembling of the circuit and all the patient and disponibility that you had throughout this project.

To my parents, thanks for allowing me to have an education and for all the patience on this rough path, all I achieved until now, and what I am set to achieve in the future is all thanks to your efforts and advice.

To my sister, thank you for all the advice and for being always there for me when I needed it. You are an example for me, someone to look up to.

To Margarida, thank you for all the help, advice and for always being there for me.

To all my friends, all the gang, you know who you are, thanks for all the help you gave me in these seven years, I could not have made it without you all. It is a pleasure to call you family, we went through everything together and we made it, lets celebrate.

To all the Refood gang, the volunteer work contributed directly to what I am today and brought the most awesome people to my life, thank you all, lets keep going.

Thank you to all other unnamed persons who somehow contributed to what I am today.

Finally, a big thank you to you Bruno. I am thankful our path came together. Whatever you are, you are my strength and the light that guides me through my path, this one is for you dude.

This work results partially of the project NORTE-01-0145-FEDER-029394, RTChip4Theranostics, supported by Programa Operacional Regional do Norte - Norte Portugal Regional Operational Programme (NORTE 2020), under the PORTUGAL 2020 Partnership Agreement, through the European Regional Development Fund (ERDF) and by Fundação para a Ciência e Tecnologia (FCT), IP, project reference PTDC/EMD-EMD/29394/2017.

NORTE-01-0145-FEDER-029394

PTDC/EMD-EMD/29394/2017

DECLARAÇÃO DE INTEGRIDADE

Declaro ter atuado com integridade na elaboração do presente trabalho académico e confirmo que não recorri à prática de plágio nem a qualquer forma de utilização indevida ou falsificação de informações ou resultados em nenhuma das etapas conducente à sua elaboração.

Mais declaro que conheço e que respeitei o Código de Conduta Ética da Universidade do Minho.

RESUMO

De acordo com um estudo realizado pelo instituto de biomateriais e engenharia biomédica da Universidade de Toronto nos Estados Unidos da América, 4 em cada 1000 pacientes sofreram de efeitos adversos provocados por fármacos. Este problema surge devido ao facto de o teste de fármacos serem realizados em animais e, posteriormente em humanos. A utilização dos organ-on-a-chip aumentam a eficácia quando se inicia os testes em humanos porque são mais representiativos do que os testes em animais. A tecnologia *organ-on-a-chip* (OOC) surgiu com o objetivo de ser possível replicar aspetos importantes da fisiologia humana e deste modo poder superar as limitações dos procedimentos tradicionais, aumentando assim a segurança e eficácia de quem os toma. Apesar da tecnologia OOC fornecer uma série de vantagens comparativamente com as técnicas convencionais, esta ainda carece de sistemas para monitorização de multiparâmetros capazes de fornecer informações à microescala durante os testes de cultura de células bem como na testagem de novos fármacos. Neste sentido, torna-se muito importante o desenvolvimento de microssensores integrados em sistemas microfluídicos para monitorizar os diversos parâmetros celulares de modo a perceber que efeitos os fármacos provocam nas células. Parâmetros como temperatura, oxigénio, pH, nível de nutrientes, entre outros, são variáveis de interesse para a perceção global do metabolismo criado pela combinação de fármacos com células de múltiplos órgãos.

Assim, o trabalho desenvolvido nesta dissertação tem como objetivo estudar e desenvolver a eletrónica de leitura e atuação de um microssensor de temperatura, baseado em *resistance temperature detector* (RTD), que será integrado na tecnologia OOC. O sistema desenvolvido para além de fornecer portabilidade e baixo custo, permite realizar leitura de vários microssensores com uma sensibilidade de 15mV/0.1°C. Foi também implementada uma componente gráfica que permite ao utilizador selecionar o sensor e acompanhar os resultados em tempo real.

Palavras-Chave: Microssensores de temperatura, *Organ-on-a-chip*, resistance temperature detetor, sistemas microfluídicos.

ABSTRACT

According to a study conducted by the Institute of Biomaterials and Biomedical Engineering at the University of Toronto in the United States of America, 4 out of every 1,000 patients suffered from drug-related adverse effects. This problem arises because the drug test mostly performed on animals and, therefore, does not faithfully question the phenomena that occur at the level of the human being. Thus, the use of these drugs can lead to complications for humans as well as damage to the pharmaceutical industry. Organ-on-a-chip (OOC) technology has emerged with the aim of replicating important aspects of human physiology and thus being able to overcome the limitations of traditional procedures, thereby increasing the safety and efficacy of those who take them. Although OOC technology provides several advantages compared to conventional techniques, it still lacks multiparameter monitoring systems capable of providing microscale information during cell culture testing as well as testing for new drugs. In this sense, it is very important to develop microsensors integrated in microfluidic systems to monitor the various cellular parameters in order to understand what effects the drugs have on cells. Parameters such as temperature, oxygen, pH, number of nutrients, among others, are variables of interest for the overall perception of metabolism created by the combination of drugs with multiple organ cells.

Thus, the work developed this dissertation aims to study and develop the electronic reading and actuation of a micro temperature sensor, based on resistance temperature detector (RTD), which will be integrated into OOC technology. The system developed in addition to providing portability and low cost, allows to perform reading of several micro sensors with a sensitivity of 15mV/0.1°C. A graphical component has also been implemented that allows the user to select the sensor and track the results in real time.

Keywords: Temperature microsensors, Organ-on-a-chip, resistance temperature detector, microfluidic systems.

Table of contents

LIST OF FIGURES

List of tables

LIST OF ABBREVIATIONS

2D – 2-dimensions

3D – 3-dimensions

ADC – Analogic to digital converter

COC – Cell-on-a-chip

GPIO – General purpose input/output

GND - Ground

I2C – Inter-Integrated Circuit

LCD - Liquid crystal display

MEMS - microelectromechanical systems

OOC – Organ-on-a-chip

PCB – Printed circuit board

PDMS - Polydimethylsiloxane

PMMA - Polymethylmethacrylate

PS – Polystyrene

RTD – Resistance temperature detector

1. INTRODUCTION

In this chapter, it will be made a contextualization of the subject, followed by the motivations and objectives of this dissertation. When it comes to contextualization, it aims at giving a little understanding of organ-on-a-chip (OOC) technology and the need for sensors to monitor them. In the follow-up, the motivation for the development of this project will be presented, realizing the reason for choosing this theme. The objectives of this dissertation will be presented and described in detail, supported by the expected results for each objective. Finally, the structure of the dissertation will be presented.

1.1 Contextualization

According to a study by the Institute of Biomaterials and Biomedical Engineering at the University of Toronto, 20% of renal diseases acquired after hospital admissions are directly related to toxicity from effects not foreseen in clinical examinations of these drugs. To understand the effects of various drugs and increase the safety and efficacy of those who use them, OOC technology is emerging for simulate important aspects of human physiology when new drugs are being developed. This technology allows recreating three fundamental aspects of human physiology: (1) the multicellular or epithelial vascular interfaces of organs, in the case of a blood vessel, lung or bowel networks, which function as barriers in tissues; (2) the organization at the level of the tissue of parenchymal cells, such as liver, heart, muscle skeleton or tumours, which are responsible for important functions of the organ; and (3) systematic interaction between organs, allowing to, more accurately, perceive all the mechanisms involved in the human physiology [1,2].

OOC technology not only incorporates various types of cells, but also engineering aspects, such as the incorporation of different types of sensors and microfluidic channels [3]. Temperature measurements are extremely necessary for most biological and chemical processes. This measurement must be effective and accurate, however, when the samples are in micro or even nano order, this task becomes quite difficult [4]. RTDs are highly linear and sensitive sensors, with a very wide temperature range between -200°C and 850°C, always depending on the material from which it is fabricated, and are therefore mostly used for

miniaturized temperature measurement systems especially due to their reduced dimensions [4,5].

This dissertation will explore solutions of temperature microsensors integrated into microfluidic platforms for in vitro testing focusing on the OOC technology, in its history and work already developed. The choice of RTD as a temperature sensor for this work compared to other sensors for the same purpose, its architecture, fabrication, measurement techniques, and its role in OOC technology will also be analysed.

1.2 Motivation and objetives

Science and technology that accurately studies and manipulates microscale fluids are called microfluidic, and OOC is a subcategory of these whose main objective is to simulate the physiological aspects of the human organ. OOC technology was considered one of the top 10 emerging technologies of 2016 at the World Economic Forum [6].

Since this is an emerging technology, although already widely used and developed, is still in an embryonic state and so there are still some shortcomings in its implementation.

One of the strands of this technology that still lacks work is the engineering around technology, in a more concrete case, the integrated sensors. This is a technology that to be functional requires sensors that allow users to monitor the environmental parameters of the cell, such as pH, oxygen levels, nutrient levels, temperature, among others. The main motivation of this dissertation is to study and develop a system of control and reading of temperature microsensors integrated on OOC to overcome the actual limitations. These microsensors were developed in the laboratory of Micro/Nanotechnologies and Biomedical Applications of the Center of MicroEletroMechanical Systems (CMEMS) of Minho University. The main objective is the development of electronic circuits to increase the reading resolution of these sensors, using low noise circuits and portable systems. This system must be able to precisely and accurately read with a resolution of 0.1°C in the range of 35°C to 45° for covering the optimal temperature of the human body. Besides, it is also aimed to develop a graphical application that allows the user to view the temperature data in real-time and change between the various sensors that can be connected to the circuit.

To accomplish this goal, some tasks must be done:

- **Development of a current source for RTD excitation**

The RTD is a temperature sensor that uses an excitation current, known and constant, to produce a voltage in its terminals, resultant from the combination of the known current and its variable resistance value at the point of measurement (Ohm law). This current value must be the maximum current that gives the best resolution and at the same time prevents the sensor from self-heating.

- **Development of low noise and portable control and readout circuit**

To provide low noise, the power source of the circuit must be independent of the power grid and this is only possible with batteries, allowing not only low noise but portability to the system. The circuit must be integrated into a PCB to contribute also to reducing the noise from wires and the electronic components that compose it, all must be low noise.

- **Development of a graphical interface**

To see the changes in temperature and results of multiple sensors, it is necessary to have an user-friendly interface that can display the values of temperature from an RTD that is connected to the system. Also, the user must be capable of selecting which sensor wants to read and save the values on a file.

1.3 Dissertation structure

This dissertation is structured in the following way:

- Chapter 1 contains the introduction, a short contextualization and the motivations and objectives of this dissertation.
- Chapter 2 present the state of art, highlighting the research about theoretical subjects and work done in microfluidic devices, OOC and temperature sensors.
- Chapter 3 presents the adopted methodology for system development.
- Chapter 4 contains the implementation of the developed system, which follows the methodology outlined in the previous chapter.
- Chapter 5 addresses all the experimental results obtained in the tests made as well as its analysis and discussion. Some improvements to the developed system are also presented.

- Chapter 6 presents the conclusions drawn from the development and validation of the system. Moreover, this chapter proposes future work to improve the system.

2. STATE OF ART

In this chapter, the theoretical component of this dissertation will be presented. Firstly, the microfluidic devices will be addressed, followed by a deeper focus on the OOC. After these topics it will be introduced the most common temperature sensors used for these applications, dedicating a sub-chapter to the RTD, the sensor that was chosen for this project.

2.1 Microfluidic systems

Microfluidics is the science and technology that process or manipulate small amounts of fluids, using channels with dimensions of tens to hundreds of micrometres. These systems involve several fields: biodefence, microtechnology, molecular analysis, and molecular biology, among others [8].

2.1.1 History

A lot of difficulties and problems in various fields contributed to the development and growth of microfluidics. After the end of the cold war, microfluidic systems were important to detect chemical and biological threats since this threat was a major concern in this era. Then, another factor was the big necessity of microanalysis, in the 1980s, in the field of molecular biology, mainly on high-throughput DNA sequencing. This process came with the neediness of systems with must higher throughput, higher sensitivity, and resolution. Microfluidics overcame these problems. At last, another major contribution to the development and growth of microfluidics came with microelectronics. Photolithography and associated technologies are successfully implemented in silicon microelectronics and MEMS fabrication. The objective was to extend this fabrication to microfluidics. This type of fabrication contributed directly to the reduction of the size of these systems. However, silicon and glass used in the first works were rapidly replaced by polymers because they are expensive and in addition to that the fabrication of the microchannels is more complex and expensive. Also, the silicon is opaque which brings problems to optical applications. Thus, microfluidic rapidly started to be fabricated in polymeric materials like polydimethylsiloxane (PDMS) [8].

2.1.2 The importance of microfluidic systems

Microfluidic systems are low-cost and miniaturized devices with a short reaction time and high throughput using a small volume of reagents/samples which allows the device to operate near its working environment. Furthermore, these devices are fabricated by easy and well-established processes. Operating close to the environment allows high performance as they are highly accurate and effective [9].

These advantages have eased the selective and effective testing of chemicals in cellular environments, therefore additionally permitting to observe in real-time the changes that this has at the physiological level of the cell, which was previously practically impossible. It is a technology with a lot of potentials that may give distinctive opportunities, for instance, for rare circulating tumour cell isolation and detection from the blood of patients, which furthers the research of cancer stem cell biomarkers and expands the understanding of the biology of metastasis [10].

2.1.3 Physics of microfluidics

Different properties are shown in the fluid flow of microfluidics [9]:

Laminar flow

The velocity a fluid stream is called laminar flow. Due to the small size of microchannels, the flow is almost always laminar. Laminar flow can be described by Reynolds number,Re, which is defined by the equation,

$$Re = \frac{\rho v D_h}{u}$$

where ρ is the density of the flow, v is the flow velocity, D_h is the hydraulic diameter of the microchannel and u is the viscosity of the flow.

Diffusion

Diffusion is responsible for mixing the different fluid flows that are in contact but never mix due to the muddy flow. This can be described by the equation,

$$t = \frac{l^2}{2D}$$

where t is the diffusion time of the molecule to diffuse over the distance l and D is the diffusion coefficient of the molecule in solution.

Capillary number

This microfluidics physics is exclusive to droplet microfluidics. The continuous phase flow that deforms the droplet is defined by the capillary number, Ca. It is defined by the following equation,

$$Ca = \frac{\eta_c v_c}{\Upsilon}$$

where η_c is the viscosity of the continuous phase, v_c is the velocity of the continuous phase, and Υ is the interfacial tension between the oil and water phases.

Weber number

Weber number is the result of multiplying the Reynolds number and the capillary number and characterizes the interfacial tension, frequently used to parametrize droplet breakup processes.

$$We = Re \times Ca$$

Bond number

Bond number characterizes the relative importance of gravity and interfacial tension. It's defined by the equation,

$$\mathrm{Bo} = \frac{\Delta\rho g w^2}{\Upsilon}$$

where $\Delta\rho$ is the density difference between the two immiscible fluids, g is the acceleration of gravity, w is the characteristic length scale, and Υ is the interfacial tension between the oil and water phases.

2.1.4 Types of microfluidics

Microfluidics can be divided into two types [9]:

Continuous-flow microfluidics

This type of microfluidics is based on a single-phase fluid in the chip. This has the objective of reducing the consumption of reagents and samples, which leads to greater speed and reproduction compared to traditional experiments. Whoever, this type has some disadvantages, like (1) the waste of fluid derivated from the overflow in the channel, (2) the

slowness in achieving uniform mixing due to the laminar flow, (3) the channel easily contaminates the fluid and the reagent, (4) the size of the devices increases with the

Figure 1 – Schematic representation of a continuous flow. Adapted from [11].

increasing of the number of parallel experiments. This technique can be seen in figure 1 [11].

Droplet microfluidics

Droplet microfluidics is based on, rather than having a constant flow of fluid, only discrete droplets are released using immiscible phases. The reaction of each droplet can be handled without the interference of reagents or the sample. Also, this type of microfluidics has a higher throughput and provides a platform to perform many reactions. There are three main techniques used in this system: (1) co-flowing, (2) T-junction and (3) flow-focusing (figure 2) [9].

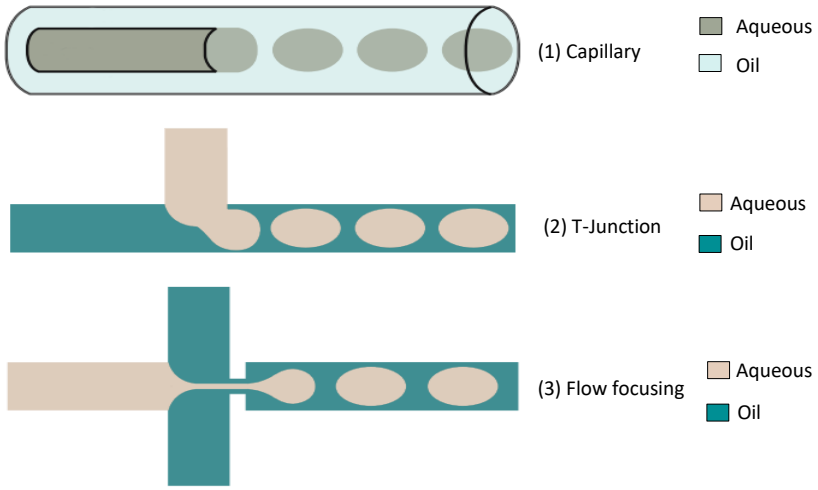

Figure 2 - Types of microfluidics techniques for droplets generation. Adapted from [8].

2.1.5 Materials for microfluidic devices

The microfluidic devices have been widely fabricated by PDMS-based soft lithography since this material is easily fabricated and easily bond through plasma treatment. Furthermore, the PDMS is a low-cost material, biocompatible with high optical transparency and has good gas permeability and high thermal stability. It also replicates nanometric characteristics from moulds fabricated by UV photolithography, which can be reused several times, ensuring reproducibility. As it has superficial treatment methods well defined enables the functionalization for the development of biosensors [12].

However, the moulding of these materials involves a largely manual process, which makes the manufacturing process difficult to automate and consequently expensive [13].

Thermoplastics, like polystyrene, PMMA, polyurethane, among others, are used to fabricate microfluidic devices, enabling high-throughput but compared to the PDMS, does not allow fabrication with high-quality. This type of material will bend around 1000 times less than the PDMS because its Young's Modulus is three times larger than the PDMS, which in some applications can be an advantage [14].

Finally, in 2008, a study proposed creating devices in paper to solve the problems of costs and the requirement of pumps. Paper is an inexpensive material that can pump the fluid itself without the need for pumps, by is wicking action, and it is accessible to anyone that has a simple wax printer. However, it has its disadvantages, namely, it is not a good material for cell manipulation because it absorbs biomolecules which can difficult the detection of some analytes, especially when they are in lower concentrations. For now, it is not an ideal solution to be used in biotechnology [10].

In conclusion, there is a need to improve the fabrication processes to reduce the total costs. It is needed for devices to be made of a material that can be rapidly prototyped, like PDMS or paper, fabricated for a low cost per unit, and where the flow can be fully controlled, stopped, and re-started.

2.2 Organ-on-a-chip

OOC is a microfluidic device specialized in mimicking the functions of human organs in vitro. It can recreate the entire cellular environment, the connections between cells and their interactions. It allows to precisely regulate the conditions where cells are growing and adapt their operation within the environment that is being recreated. Thus, regulates all parameters and optimizes the cell culture microenvironment [16].

Preliminary testing of drugs before they are available to humans is the most important process, both on the consumer side, to ensure that they do not suffer from serious side effects, as well as on the pharmaceutical industries side, as these tests incur high costs and it is imperative to assure the safety of the consumer.

The development of new drugs goes through a stage of animal testing, which sometimes produces a high failure rate because they do not replicate human physiology very accurately. In addition, they are time-consuming processes and have ethical issues that greatly limit their use. So, the test in animals has been complemented by 2D cell cultures in vitro [1,3]. However, in vitro models, reveal one major disadvantage compared to the in vivo methods, they cannot, most of the time simulate the complex cell-cell and cell-matrix interactions crucial for regulating cell behaviour in vivo. Despite that, they are useful for studying the molecular basis of physiological and pathological responses. The problems with testing in 2D models or animal-based models have generated sizeable interest in the search of human-based tissue-like constructs for improving the disease modelling and drug and chemical testing, increasing their effectiveness and reducing economic losses from the lack of effectiveness [17].

Since the 90s, several microfluidic technologies have been applied to in vitro systems. Microtechnology has opened doors to OOC technology for several reasons: the fact that makes it possible to implement small electric and fluidic circuits to be integrated into miniaturized devices. They also allow greater precision and facilitate the delivery of essential nutrients for cell growth, due to their laminar nature, so the gradients are of high concentration due to a shorter diffusion length. Finally, as the last advantage, the shear stress applied to the cells can be controlled and minimized. In a way, all these advantages allow the creation of a well-controlled environment in the in vitro cultures within OOCs, and thus

enhancing the results obtained so that they are as close as possible to the response of a human organ [18].

Andre Kleber was the first to study and talk about cells for in vitro disease study [19]. Since then, several microfluidic devices have been developed, replicating the human biological conditions such as blood cells, muscles, bones, liver, brain, intestine and kidney. The major milestones and establishment of OOC technology can be seen in figure 3 [19].

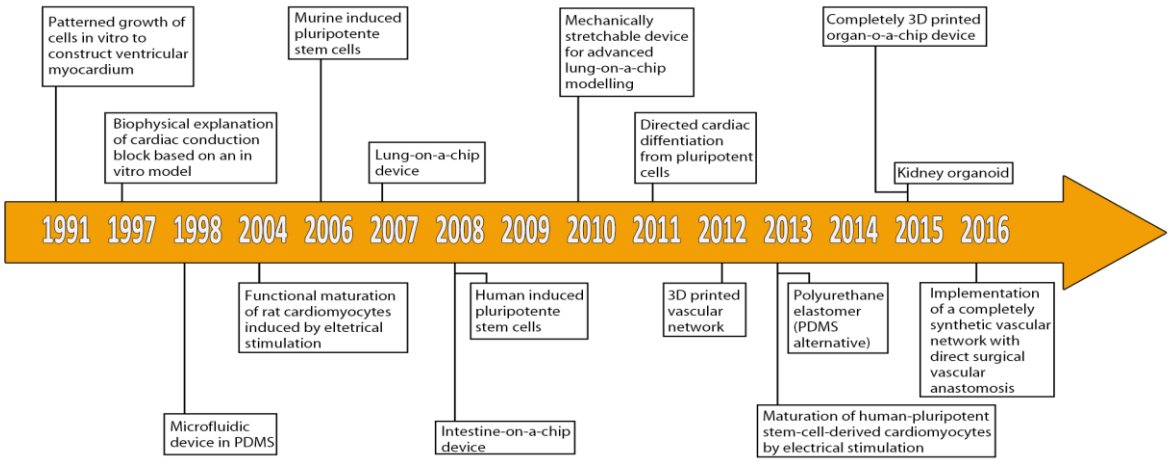

Figure 3 - Major milestones on OOC technology. Adapted from [19].

The term OOC was proposed by Doctor Donald Ingber and his team, who developed a microfluidic chip to replicate the functions of a human lung in 2010 [17]. Since that, multiple OOC were developed and their evolution is presented, in figure 4 [16].

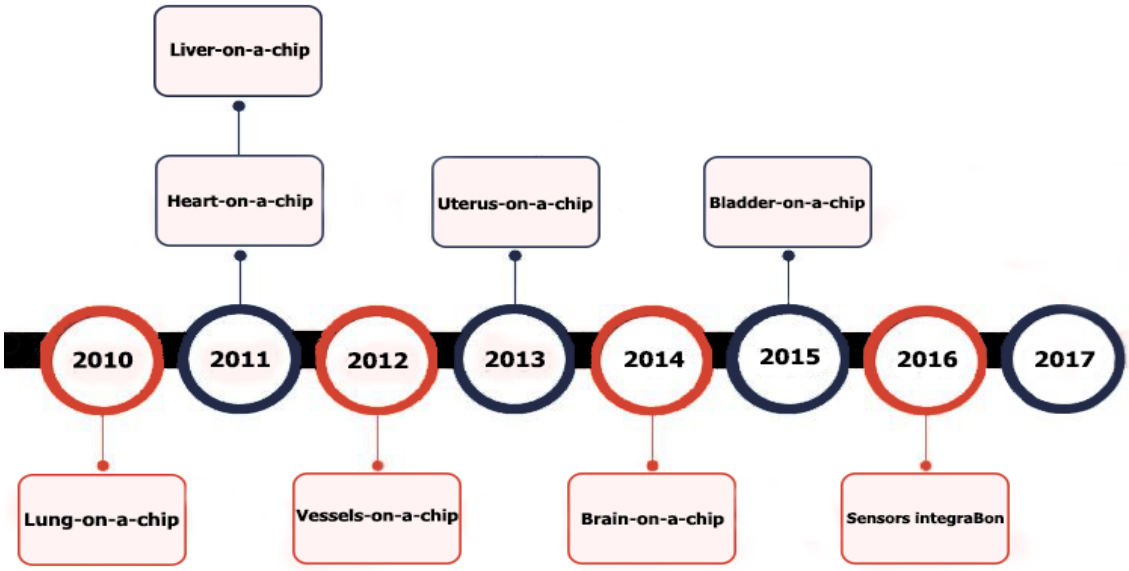

Figure 4 - OOC devices discovered, by chronological order, until 2016. Adapted from [16].

2.2.1 Main components of OOC

The OOC involves four key components [3]:

- **Microfluidics –** Microchannels that permit interaction with the cell and manage the environment.
- **Living cell tissues –** The living organoids that are going to be tested.
- **Stimulation or drug delivery –** Channels to drugs delivery and stimulate the microenvironment.
- **Sensing –** Electronic microsensors for monitoring the effects of the drugs in the microenvironment and cells.

Furthermore, these culture systems need management of external and internal cell environments. OOC combined with micromachining and cell biology will manage external parameters [3].

- **Fluid Shear force -** Microfluidics allow, through micro-pump perfusion, to implement a dynamic culture. By that, is easy to deliver nutrients to the environment and in the same way, it enables the discharge the wastes from the environment.
- **Concentration gradient -** The fluid acts, at the microscale level, as a streamline flow, controlled each spatially and temporally, leading to a stable gradient of nutrients, drugs, and others.
- **Dynamic mechanical stress -** This mechanical stimulation, that mimics the day-to-day organ pressure such as blood pressure, lung pressure, and blood pressure, is considered a key determinant of differentiation during physiological processes. Microfluidics allows the use of elastic membranes to create these pressures, keeping mechanically stressed tissues like blood vessels, bone, muscle, and cartilage.
- **Cell patterning -** Cell pattering is a must-have feature of this type of technology because is important to simulate the interactions of this complex and ordered arrangement of multiple cells presented on the human body. Cell patterning is permitted by surface modifications, templates and 3D printing.

2.2.2 OOC devices

Various OOC technologies have been developed and tested over the years, specifically:

Liver OOC

The first to design a liver-based system were Kane *et al.*[20]. This system consisted of microfluidic pores where rat liver cells and 3T3-J2 fibroblasts were co-cultured to mimic an airway interface. The main applications of Liver OOC are the study of drug metabolism, hepatotoxicity, particle-cell interactions, among others.

Lung-on-a-chip

The first lung-on-a-chip model was designed by Hugh *et al.*[21]. This model replicated the respiratory motion through a vacuum leading to mechanical stretching and the formation of an alveolar-capillary barrier.

Kidney OOC

Jang *et al.* [22] designed and produced the first kidney OOC. The channel could replicate the urinary cavity and capillary lumen of the glomerulus.

Heart-on-a-chip

Grosberg *et al.* [23] designed and produced an elastic film with a textured surface and implanted neonatal rat cardiomyocytes on the membrane to form a muscle membrane to mimic the functions of the myocardium. It is mainly used in cardiovascular toxicity and drug screening tests.

Intestine-on-a-chip

Imura *et al.* [24] developed chips to simulate the intestinal system, consisting of a glass slide, a permeable membrane and a PDMS sheet containing channels [4].

Multi-organs-on-a-chip

Van *et al*. [25] were the first to combine liver and intestines in a microfluidic device. The intestine and liver slices functioned on the chip demonstrating their applicability and was possible to study the organ interactions, such as the regulation of bile acid synthesis [3].

2.2.3 Economic impact

Some studies indicate that around 50% of drug failures in the testing phase are due to their lack of efficacy and 15% to 25% are due to safety problems. Thus, OOCs can be very important in reducing the costs of research and development of pharmaceutical industries since they are very close to the expected and real results in the human body, reducing the percentage of failure and consequently the costs of research. In a study performed by N. Franzen *et al.* [26], it is stated that the costs per new drug vary greatly between US$330 - US$2760 per test, depending on the drug and the phase of research and testing. More say that a cost reduction of 10-26% is expected in a general scenario by using OOC devices, resulting in estimated savings up to US$169milion and US$706million per new drug that reaches the market [27].

Finally, the complexity of the OOC models was improved with the final objective of creating a human-on-a-chip, a full-body composed of multiple OOC devices in place of human organs. However, this technology is still very far away even with the clear advances of this technology, still has many points to improve, being yet in an embryonic phase. High-cost, non-reusable equipment makes this technology have a high implementation cost. As more OOCs are implemented, the systems become more complex, the functionality is higher which provides better efficacy of these models. However, they require accurate monitoring systems, like temperature measurement to monitor the cell environment and to assess hyperthermia treatments

2.3 Temperature Sensors

There are several types of temperature sensors, but the most used are thermocouples, thermistors and RTD. The main characteristics of each type will be presented below.

Thermocouples

Thermocouples are temperature sensors based on thermoelectric effects, such as the Seebeck, Peltier, or Thomson effect. This type of sensor is fabricated from two different materials forming a temperature-sensitive electrical junction. When this junction is exposed to a temperature change, an electrical voltage is created which can be correlated with the temperature (Seebeck effect). The electrical potential between the two junctions is called Seebeck voltage [28].

The Peltier effect is the production of a thermal gradient between the two junctions when an electrical voltage is applied in the ends. This gradient happens due to the flow of current which cause an emission or absorption of heat in the junctions [29].

The Thomson effect, unlike the two previous effects, happens when the conductive material has two points with different temperatures and is measured the electrical voltage between them resulting from that difference of temperature between the two points [30].

Since thermocouples involve the joints and all extensions of wires, to ensure the proper functioning of the sensor, the temperature gradient must be the same in all these components. Failure to comply with this characteristic can lead to different gradients which leads directly to errors and misrepresented Seebeck voltage values and, consequently, to non-real temperature values. This distinguishes thermocouples from other sensors since it doesn't give temperature but a temperature gradient. Thermocouples are used in various applications, and for temperatures above 500°C, they are the only ones that measure temperature in contact with the system [31].

These sensors are simple, robust, and cheap. They do not require external energy, have a large temperature range, and can be manufactured with several designs. On the other hand, they hold a nonlinear response, have little sensitivity and have a small and low stable output voltage [32].

Thermistor

The thermistor is a semiconductor-based temperature sensor that can be subdivided into two types:

- Negative temperature coefficient (NTC) when the value of electrical resistance decreases with the increase of temperature;
- Positive temperature coefficient (PTC), the value of electrical resistance increases with increasing temperature [28].

Although they are non-linear sensors, which makes it difficult to accurately measure temperature, the thermistor is the most commonly used sensor in the automotive industry and on quotidian devices due to its low cost, high sensitivity and the possibility of being manufactured in various shapes and sizes [23].

The thermistor is a fast response sensor, with an output of high values and with few losses in its resistance resulting in few measurement errors. However, it contains a small temperature measurement range, is externally powered, is non-linear, is quite fragile and is affected by self-heating [28].

Resistance temperature detector (RTD)

The RTD is a sensor composed of a conductive material, usually, platinum, which needs a current that flows through the sensor and generates an electrical potential between its terminals. Its resistance value increases with the increase of the temperature, which makes its output value increase [34].

RTD is the most stable sensor of the three presented, has good linearity and is the most accurate. It is a pure conductor and is the sensor that best suits implementations in industrial contexts because they can cover all the necessary characteristics and at the same time are the most accurate making their calibration systems cheap and simple, since this is usually used for short temperature ranges [35]. Furthermore, this sensor demonstrates greater long-term stability[36]. More details about RTD can be found in section 2.5.

In conclusion, these three sensors have their vantages and disadvantages. The thermocouples are simple, rugged, inexpensive, do not need external power, have a wide temperature range, commonly -270°C to 1800°C, and come in various assembles, but on other

hand have a nonlinear response, small sensitivity, small output voltage, require cold junction compensation and are least stable. The thermistor is a fast response sensor, has a high output and minimal lead resistance but needs an external power or voltage source, is non-linear, very fragile and suffers from self-heating errors. The RTD is the most stable with good linearity and accuracy (0,01°C) but has low sensitivity, around 0,00385 Ω/Ω/°C for platinum sensors, it is also externally powered with a current source, it is more expensive, has a small output resistance and also suffers from self-heating errors. However, the RTD are easier to miniaturize and fabricate into the microfluidic devices and with suitable amplification and filtration electronic circuits, a high sensitivity response can be obtained [31,36].

In the development of a sensor, it is important to take into account certain characteristics appropriate to the desired application [32]:

Operation interval

In the operation interval, the temperature limits that the sensor reads, lower and upper, are defined. A longer interval can sometimes provide a lower sensor's linearity and sensitivity.

Linearity

Is the capability of the sensor to respond linearly to all the changes of temperature through all the operation range.

Sensitivity

It is said that a sensor is more or less sensitive depending on the change in its output value when the temperature changes, that is, with a small temperature change, the more variability there is in the output value, the more sensitive it is the sensor.

Response time

When a temperature change occurs, the time it takes for the sensor output to change its value is given with the response time of the sensor.

Stability

This characteristic is defined by the sensor's ability to maintain the same result at the output when it is under a stable temperature.

Efficacy

The effectiveness of the sensor is given by the environment that surrounds it and the circuits where it is implemented. To be more effective it is normally needed good wiring, good grounding throughout all circuits, noise filtration, among others.

Durability

The durability of the sensor is the capability of the sensor to operate in the same environment for some time, normally decided by the manufacturer. This characteristic is usually related to the material that composes the sensor and its encapsulation.

Requirements for conditioning signal

All sensors will have various signal conditioning requirements such as amplification, cold-junction compensation (thermocouples), filters, excitation (RTD and thermistors), offset error adjustment, scaling to temperature units, lead resistance correction, channel-to-channel isolation, open thermocouple detection (thermocouples only).

Costs

In all projects, it is important to denote the costs, sometimes a cheaper sensor will satisfy the needs of the project, as it will probably need less surrounding material like wiring, signal conditioning or even assembly costs. However, some applications need more complex sensors and thus optimized manufacturing, which can increase the final cost. Nevertheless, the level of integration or the sensitivity required may justify a higher cost.

2.4 Temperature measurement in microfluidic devices

Several works about temperature measurements in microfluidic systems have been studied and implemented. In the first example, it is presented a nanoneedle to measure the temperature of single cells. This system studies the possibility of a flow of water to move the cells against the nanoneedle with enough amount of force to permit the nanoneedle to penetrate the cell without damage. An electrical voltage is applied to the nanoneedle and it is measured the output current for the conversion of temperature, however, the study was only simulated and not implemented, the results were promising [38].

It is increasingly important to analyse the behaviour of cells, but it is also necessary to be careful to not damage them. There are cells from diseases such as cancer, which reveal an

increase in temperature which makes it important to study intercellular temperature. To measure cell temperature, many attempts were made, successfully and with high levels of sensitivity, but the materials used in these measurement systems proved to be a critical disadvantage because of their high toxicity within the cell influencing their development. These phenomena occurred when temperature sensitive-materials were used to measure the temperature of cells, such as quantum dots, that are used as nano thermometers [39], nanoparticles, that are connected with other nanoparticles and together act as a molecular spring and with the variation of the temperature its extension changes and that extension is used to measure the temperature [40], and thermosensitive materials [41].

Nanoneedles followed, accompanied by material with properties that are affected by temperature change. In the study of Binsilm *et al.* [38], a nanoneedle microfluidic system was presented. The based material used in its fabrication was the tungsten and the sensor showed to have a positive temperature coefficient of temperature (TCR) with the increase of temperature. Fabricated in Y shape allowed the nanoneedle penetration in the cell to cause minimal damage to the cell. The output of this sensor is given in the current form, and it was obtained a resolution of 0.02°C which translates in variations of 50nA.

In a study by Chunyan Li *et al.* [42], is presented the development of a smart microcatheter with several integrated microsensors, such as a temperature sensor (RTD), flow rate sensor (hot-film anemometry) and glucose biosensor (amperometric sensor). The temperature sensor was fabricated in titanium gold (Ti/Au) deposited in a polymeric and flexible substrate. A precise and linear response concerning temperature was demonstrated using the fabricated RTD. Furthermore, the authors showed that the fabrication process of microcatheter with integrated microsensors is very simple and suitable for low-cost mass production.

Another approach of temperature sensors in the microfluidic system was related by Naoki Inomata, et al. [43]. This approach was based on a pico calorimeter that uses a resonator to detect the temperature variation in the sample by frequency tracking of the resonator. The system has a heat guide that conducts the heat to the sample and the resonator is kept in vacuum. The change of temperature makes the resonator vibrate and that vibration frequency was translated in the variation of temperature in the microfluidic channel. Was achieved a resolution of 5.2 pJ in the fabricated sensor.

Microfluidic devices are not only used in medical experiments. In the works of Schmitt *et al.* [44] was proposed the implementation of an intelligent microfluidic temperature indicator to precisely predict the expiring date of the food on the package. The idea goes through a smart package with passive sensors that, based on the temperature and time that food is packaged, demonstrates a more real expiration date than conventional ones printed at the time of packaging that is estimative. Sensors that already exist are usually on the outside of the package and use read circuits that do not make it very easy to read. This study proposed a sensor with wireless reading. The sensor is composed of a capillary with a rectangular cross-section with two electrodes placed in opposite walls to obtain a plated capacitator. Non-toxic fluid is used with high viscosity that will melt, reducing the viscosity, with the increase of temperature, entering the microcapillary, and increase its viscosity with the decrease of temperature, decelerating the fluid and stopping it. The distance that the fluid travelled will be related to the capacity between the two electrodes, which increases proportionally with the increase in temperature.

Finally, an RTD sensor was bonded together to the surface of a PDMS based thermoelectric cooler in a work of Oiler *et al.* [45] for atherosclerosis studies. As the previous works that used hot-wire anemometers, although having high sensitivity and being robust, had a limitation in flow properties measurement at cell level because it was proven that damages the cells. It is important to understand the blood flow in atherosclerosis studies because this disease affects directly the blood vessels bifurcations and it is detected by studying the shear stress that is directly correlated with the flow rate. The thermoelectric cooler was fabricated in PDMS and the RTD was bonded to the surface of the device, this allowed each time that the flow was increased, the temperature sensor detected that increase by changing its value of temperature. This proves that it is possible to use the RTD in a thermoelectrically cooler to measure the flow rate of blood.

2.5 Temperature microsensors based on RTD

Measuring temperature with conventional sensors such as thermocouples and thermistors are successful in samples in the order of millimetres, but when advancing to smaller samples these sensors are more difficult to integrate, as an example, into microfluidic devices. Several approaches for cell culture temperature sensing have been explored in

previous works such as commercial PT-100 RTDs [46], fluorescent polymeric thermometers [47] and commercial T-type thermocouples [48]. However, these solutions are not very compact for integration in microfluidic devices or present a poor resolution. The advances in microtechnology have allowed the development of miniaturized temperature sensors based on RTDs which can be integrated within microfluidic devices, as proposed in this dissertation [4].

2.5.1 Characteristics

To characterize the RTD's, some details about it should be specified [49]:

Type of resistive material

Most RTD is fabricated with platinum, although other materials as nickel, aluminium, copper can be used. Platinum is the preferred material since has higher linearity and sensibility.

Temperature coefficient

To convert the sensor output values to temperature, it is necessary to parameterize the temperature coefficient which represents the change of resistance per unit of the temperature of the resistive material from 0°C to 100°C (freezing and boiling temperatures of the water, respectively). The temperature coefficient declared by the IEC (International Electrotechnical Commission) in 1983 for the platinum was 0.00385 ohms per ohm degree centigrade. This value is accepted worldwide when using platinum RTDs.

Nominal resistance

This feature is the temperature that should be expected for various temperature values. 100 ohms is the standard IEC at 0°C for PT100 but there are other nominal resistances available (PT500, PT 1000, and others).

Temperature range of operation

As its name implies, it is the temperature range where the sensor operates. This value varies with its configuration and fabrication methods.

Dimensions and size restrictions

The resistive element must fit inside its protective encapsulation, so its most important dimension is the outer diameter. In this case, the RTD are easy to miniaturize facilitating its integration.

Precision

This specification is given according to the IEC 751 for platinum RTD's as we can see in table 1, divided by two classes (class A and class B) following DIN 43760 requirements for accuracy.

Table 1 - Permissible deviations from theoretical platinum RTD values. Adapted from [34].

Temperature °C	Class A		Class B	
	Deviation		Deviation	
	Ohms	°C	Ohms	°C
-200	±0.24	±0.55	±0.56	±1.3
-100	±0.14	±0.35	±0.32	±0.80
0	±0.06	±0.15	±0.12	±0.30
100	±0.13	±0.35	±0.30	±0.80
200	±0.20	±0.55	±0.48	±1.30
300	±0.27	±0.75	±0.64	±1.80
400	±0.33	±0.95	±0.79	±2.30
500	±0.38	±1.15	±0.93	±2.80
600	±0.43	±1.35	±1.06	±3.30
650	±0.46	±1.45	±1.13	±3.6

Response time

It is the time that the sensor takes to respond to a change of temperature and provide a stable value.

Self-heating

This is a parameter that is very important to be aware of because it translates in perturbations on the values on the reading. As these sensors need a current of excitation to operate, that value must be chosen and parameterized so the sensor never enters in self-heating. This error is translated into °C/mW.

Wire configuration

The electrical connections for the excitation and reading of the RTD sensors add electrical resistance that is summed up to the resistance of the sensor. In this way, when

accuracy is important, the wire configuration needs to be considered to minimize that influence.

2.5.2 Fabrication

There are RTD's fabricated with conductive wire wrapped in a glass or ceramic core, however, the miniaturized RTD's are usually based on resistive thin-film of platinum, nickel, or aluminium. Platinum RTD's are the most accurate because they demonstrate greater stability over time. Temperatures can be measured in a range of -189°C to +962°C with a maximum accuracy of 0.001°C [36]. The thin profile of the RTD allows it to be fabricated in a plane wall with a thickness of few nanometers and thus, can be easily integrated into microfluidic devices. Usually, glass or PDMS are used to close the microfluidic channels and RTD can be directly fabricated onto this substrate. The RTD is fabricated by thin film vacuum deposition techniques and their standardization is carried out by photolithography techniques and lift-off process [44,45].

First, it is necessary to realize that the fabrication of nanomaterials and nanostructures is performed in an extremely clean environment called a clean room, in which there are few particles and specialized equipment for three basic functions: (1) Thin film deposition; (2) Patterning; (3) Etching.

The thin film deposition requires a vacuum environment in the order of 10^{-6} torr or 1.3×10^{-4} Pa to ensure that any impurities or contaminants are not present in the deposition chamber. The materials to be deposited must be of high purity, typically 99.9999% or higher.

The three most common thin film vacuum deposition techniques are:

Thermal evaporation

Thermal evaporation uses heat to evaporate the source material of high purity from solid material to gas. The gas atoms travel through the vacuum inside the chamber and when these atoms reach the subtract, they condense and form a thin film on the surface. Metals and dielectrics can be deposited using this technique but are most commonly used to deposit metals because their boiling point is much lower and their deposition rates are more stable. This process is completely automatized, a computer controls the temperature inside the chamber and the thickness of the thin film, it just needs the user to insert at the beginning of the process the thickness desired and the limit of temperature [52].

Electron beam evaporation

Electron beam evaporation is similar to thermal evaporation. It also uses heat to make the evaporation of the high purity material and is performed inside a vacuum chamber. The major difference is the source of heat. A beam of electrons is responsible for heating and consequent evaporation of the material to be deposited [53].

The electron beam allows the heating of a metal filament until about 2500°C. At this temperature, the electrons are very energetic and some of them leave the surface of the filament and are accelerated in direction of the source material with the help of a high voltage electrode. A group of magnets lead the electron and focus the beam to the source material [53].

One of the advantages of this technique is that it allows being deposited different materials on the substrate without opening the chamber because the electron beam is well confined in space, it heats only a small area of the source material allowing other source materials to be in the chamber to be evaporated sequentially. The source material is put inside the chamber on the crucible [53].

Systems that hold four materials are very common and they are called the four-pocket hearth. Four crucibles fit into the hearth, and each crucible can hold a different source material. So that it can have up to four layers of different materials deposited without breaking the vacuum. The hearth is a rotated holder of copper which is water-cooled. The water cooling prevents the crucible material from melting and mixing with the source material or with the hearth itself [53].

Sputtering deposition

Sputtering is a different process compared to the other two types because it does not use evaporation. Instead, uses energized atoms that reach the source material (target) to be deposited on the substrate. These energetic atoms hit the target and propel the atoms of the source material out of the target and into the vacuum system. Some of these atoms reach the substrate that is arranged on the top of the vacuum chamber and deposit. These energetic atoms used in the process are created by plasma. The argon is the gas used to form plasma because it is an inert gas and will not result in unwanted chemical reactions during the process [54].

When the gas is in the chamber, a high electrical voltage is applied to the target. This high voltage is strong enough to remove an electron from the argon atoms causing it to become ionized and as the source material is negatively charged, the argon atoms will react with these atoms individually by removing them from the target material and peppering them in various directions, including toward the substrate [54].

Photolithography

Photolithography is an indispensable step in the fabrication of thin film-based RTD. This technique is responsible to transfer the desired pattern of the sensor to a photoresist material which is used to protect selected areas during subsequent etching or deposition processes. It uses ultraviolet light to transfer the geometric pattern from an optical mask to a photoresist deposited on the substrate [55].

3. METHODOLOGY

In this chapter is presented the methods and the validation of a temperature sensor based on RTD. All the procedures inherent to the development of these systems are defined. The general requirements will be portrayed in the following.

- Reading resolution of 0.1°C, in the range of 35°C to 45°C;
- Low noise circuit;
- Real-time and in situ monitoring;
- Display the collected data in graphical form;
- Compact size;
- Portable system;
- Capability to read more than one sensor.

The main goal of this dissertation is the development of a system to measure temperature changes in OOC with a resolution of 0.1°C in a range of 35°C and 45° C. This range of temperature values covers the typical human body temperature, around 37°C, where the human cells typically grow and it also can be used in studies of hypo (35°C) or hyperthermia (42°C). To achieve this goal, the noise in the circuit must be minimum because in low signal systems like this, every perturbation, even if it is minimal, is going to have a big impact on the signal and, consequently on the values that are read and converted. At last, the values that are read and converted are going to be displayed in graphical form to be easy for the user to follow the temperature transitions of the environment where the sensors are inserted. A resolution of 0.1°C is crucial for detecting, as an example, an exothermic reaction resulting from the interaction of the cells with drugs. Furthermore, the system must be portable and compact with the capability of reading multiple sensors. The portability and the reduced size will allow the system to operate inside of equipment with small dimensions, like incubators where the levels of oxygen and carbon dioxide are controlled. The RTD sensors will be integrated into microfluidic devices, and thus, the developed system must be able to perform automatic, real-time and in situ temperature measurements.

The control and the reading system developed in this dissertation was divided into different parts for a better understanding of the system. Furthermore, it simplified troubleshooting if something is not working or needs to be improved/changed.

In figure 5 is showed the block diagram of the system comprising three main parts: reading circuit, data acquisition and data visualization.

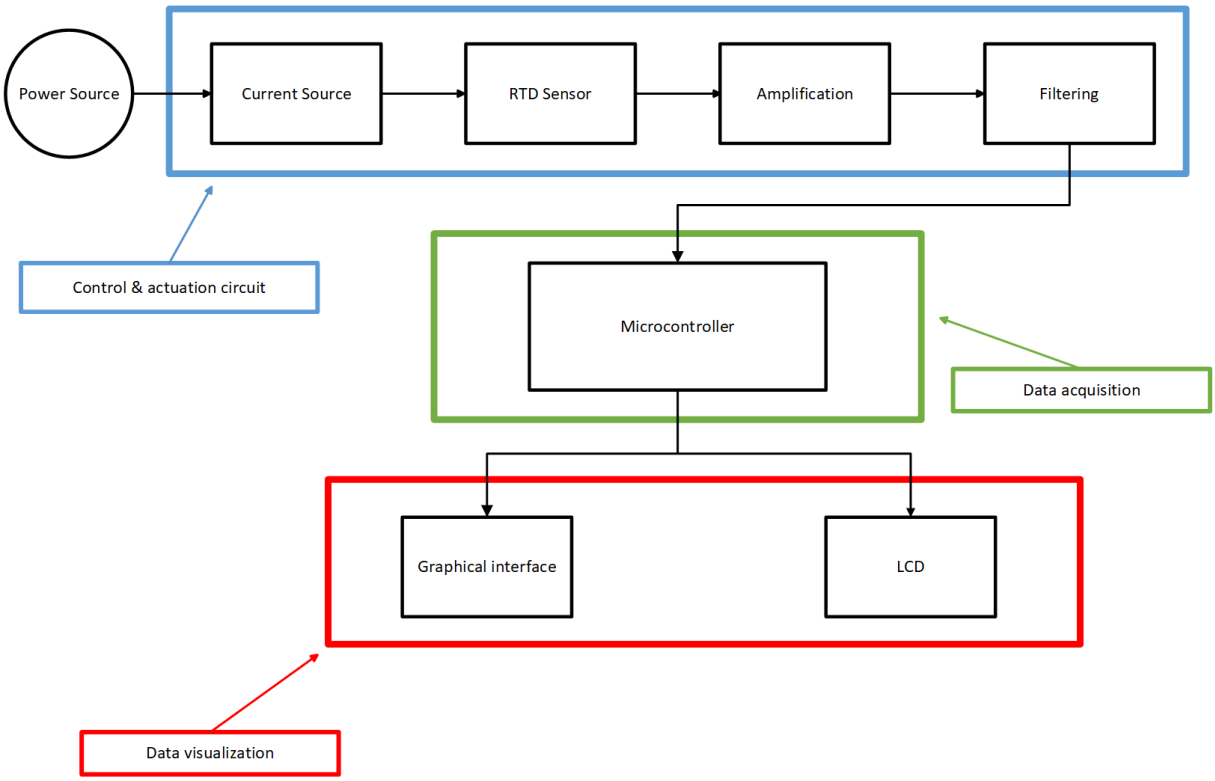

Figure 5 - Block diagram of the implemented system.

3.1 Development approach

3.1.1 Measurements circuits and wiring configurations

Callendar-Van Dusen equation (CVD) relates the resistance of platinum RTD with temperature. Equation 1 is used to calculate the resistance for temperatures below 0°C and equation 2 is used to calculate the resistance for temperatures above 0°C [6].

For T < 0: $R_{RTD}(T) = R_0 \cdot \{1 + (A \cdot T) + (B \cdot T^2) + [(C \cdot T^3) \cdot (T - 100)]\}$ (1)

For T > 0: $R_{RTD}(T) = R_0 \cdot \{1 + (A \cdot T) + (B \cdot T^2)\}$ (2)

R_0 is the resistance of RTD at 0°C and the coefficients of the equation are defined by IEC-60751 with the following values:

- $A = 3.9083 \times 10^{-3}$
- $B = -5.775 \times 10^{-7}$
- $C = -4.183 \times 10^{-12}$

The conversion of temperature can be done also by relating the temperature coefficient of the material, which is the variation of resistance per degree of temperature, that the sensor is fabricated with the resistance at 0°C of the sensor and the value of resistance that it is given at the terminals at the moment of the reading. The equation is the following:

$$R = R_0 * (1 + \alpha T) \tag{3}$$

which solved in order of the temperature, looks like this:

$$T = \frac{R}{R_0 * \alpha} - \frac{1}{\alpha} \tag{4}$$

where α is the temperature coefficient of the material, R_0 is the resistance of the sensor at 0°C and R is the resistance given by the sensor at the time of the reading, normally it is converted from the Ohm Law:

$$R = \frac{U}{I} \tag{5}$$

where *U* is the output voltage given by the sensor and *I* is the excitation current defined and known. In table 2, it can be seen the temperature coefficient of the most used materials for this type of sensor.

Table 2 - Temperature coefficient values for the more common materials used in the fabrication of RTDs.

Material	Temperature coefficient (Ω/°C)
Copper	0.00386
Aluminium	0.00429
Platinium	0.00385
Silver	0.0038
Tungsten	0.0045

To scale a measurement circuit of an RTD is necessary to have some considerations. In the first instance, the interval in which the RTD will operate should be well defined because this will also define the interval in which the RTD resistance values will be. This will help define the excitation current, gain and possible resistance of reference [6]. The excitation current should consider the self-heating of the RTD, that is, it must be chosen so that the RTD does not heat up, preventing the output from being influenced by this effect. Interim Digital-Analog Converts (IDAC's) are typically used, programmed and can charge currents from 10 to 2000µA however excitation currents should not exceed 1mA. RTD's self-heating coefficients of thin film and rolled wire are 25mW/°C and 65mw/°C, respectively [6].

The third phase will be to choose the gain for the ADC since it mostly has a minimum and maximum input voltage. Finally, the entire circuit must be assembled and tested to determine whether it falls within the range in which the RTD will operate [6].

There are three types of wiring configurations for RTD that help to reduce the measurement error generated by the lead wires:

Two-wire configuration

Each end of the RTD is connected to two wires. In this configuration, the wire resistance cannot be separated from the resistance of the RTD which adds an error to the resistance measurement that cannot be eliminated without the help of other circuits. This type of configuration is typically used when RTD accuracy is not important or the conductive wires are short. It is also the cheapest configuration [6]. As can be seen in figure 6, the total resistance can be defined by (6)

$$R_{Total} = R_{Rtd} + R_{wire1} + R_{wire2}.$$

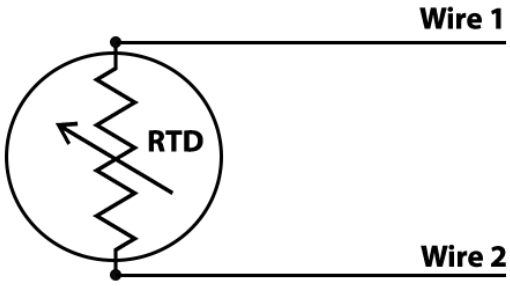

Figure 6 - Schematic representation of the two-wire configuration.

In this configuration, lead wires errors are significant since the current flows through the two conductors generating resistance in series with the sensor. The output of the sensor is measured on the same wires and add the resistance of the RTD and the conductor creating reading errors [56].

Comparing this configuration to three wires and four wires, the costs of adding more wires are extremely higher, especially when dealing with industries with various monitoring and control points [56].

A cheaper solution based on a two-wire configuration was analyzed and implemented by Wei Li *et al.* [56] that approximates the results to other configurations, reducing errors derived from the lead wire resistance. The system consists of a circuit that can be divided into four different areas: (1) an area where the RTD is; (2) an area in the same environment with a Zener diode; (3) an area with the conductors; (4) a final area of control and monitoring of the system. This system demonstrated final results with errors around 0.3°C which translates into a percentage of about 0.14% of error.

Three-wire configuration

In the three-wire configuration, one of the two ends is connected to a wire and in the other end two wires are connected, one of which is used only for reading the output and the other two for the excitation current to flow. In these configurations, the lead wire resistance can be drastically reduced but will not be eliminated, and there will be still some error in the sensor resistance value [6]. As can be seen in figure 7, the total resistance can be defined by (7)

$$R_{Total} = R_{Rtd} + R_{wire2} + R_{wire3}$$

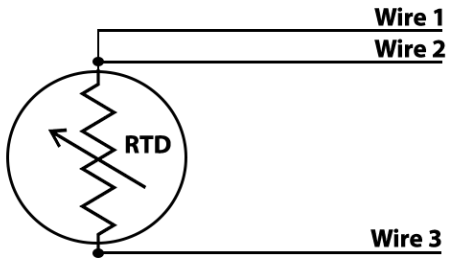

Figure 7 - Schematic representation of the three-wire configuration.

Wire 1 is where the current source is connected and the resistance of wire 2 is nearly zero because the current flow by wires 1 and 3,

$$R_{Total} = R_{Rtd} + R_{wire3} \, . \tag{8}$$

As a result, it is necessary to reduce this error caused by the lead wire resistance, which although it is already smaller than in the previous configuration, still exists and can be eliminated without adding another wire. A proposal for a three-wire interface with an adjacent Wheatstone bridge was analyzed by T. Junsing *et al.* [57]. This approach is an alternative to the four-wire configuration and, consequently, obtaining a solution with the same result and more into account, since the cost of implementing the bridge is practically negligible. Figure 8 shows the configuration with the Wheatstone bridge:

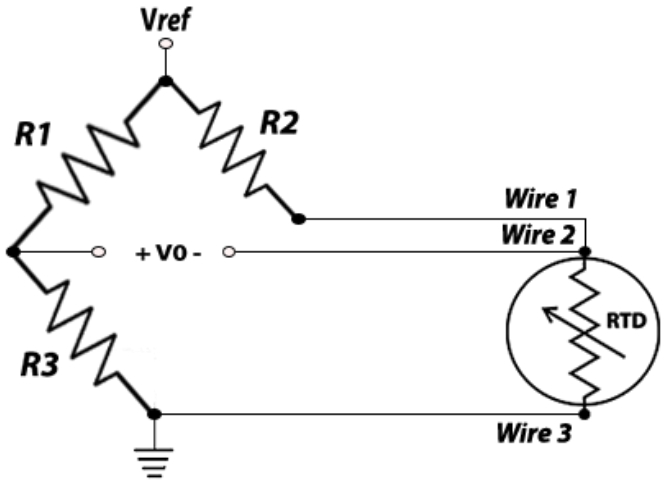

Figure 8 - Schematic representation of the three-wire configuration with Wheatstone bridge compensation. Adapted from [57].

In the end, the circuit was found to be measuring errors below 0.2%, although the circuit was only simulated and these results are only theoretical, it was considered that this solution is feasible [57].

Four-wire configuration

In this configuration, each end of the RTD will have two wires connected, in which one of the pairs will be to the excitation current to flow and the other pair are used for measuring the output of the sensor. Here the resistance is measured with high precision since the excitation current is flowed by different wires from the measuring wires, avoiding voltage drops in the measuring wires. In this way, the resistance read comes exclusively from the

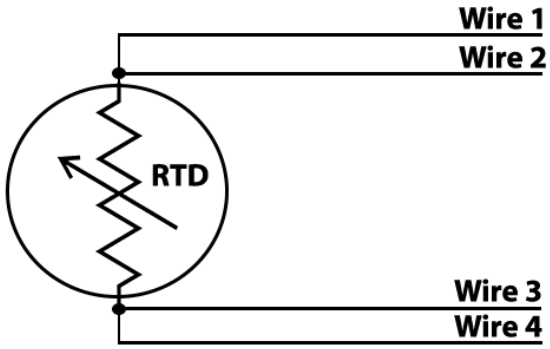

Figure 9 – Schematic representation of the four-wire configuration.

sensor [6]. The configuration can be seen in figure 9.

The total resistance is given by

$$R_{Total} = R_{Rtd} + R_{wire2} + R_{wire3} + R_{wire4}. \quad (9)$$

Normally the current is flowing by wire 1 and 4 and wires 2 and 3 are used for the output of the sensor and their value of resistance is nearly zero, it's possible to conclude that

$$R_{Total} = R_{Rtd}. \quad (10)$$

This type of configuration does not suffer from lead wire resistance errors and is therefore implemented without the need for any type of complementary circuits such as the previous configurations. So, this configuration was chosen for the implemented system as it is the one that offers better noise reduction and as the sensor will be implemented close to the operating environment, the costs related to the wiring of the sensor are low.

In [58] an installation of a sensor using the four-wire configuration for geothermal studies was addressed. Since it is an application where the sensor is installed at about 100m depth, this makes it impossible for the sensor output values to be read on site. It is necessary to use conductive wires for the values to be read remotely. These wires will have a resistance that is associated with them what causes the results to be changed and are not real, so the four-wire configuration for this application was chosen. As expected, it was concluded that there were no fluctuations or measurement errors derived from the resistance of the lead wires and all the values read on the sensor were the real ones.

3.1.2 Fabricated RTD

The temperature microsensors used in this dissertation were developed in previous works of some researchers in the laboratory of Micro/Nanotechnologies and Biomedical Applications of the Center of MicroElectroMechanical Systems (CMEMS) in partnership with the International Iberian Nanotechnology Laboratory (INL) where they were fabricated. More detail about the fabrication process and characterization of the temperature RTD microsensors are described in [59].

After some comparison studies, platinum was selected to fabricate the RTD, since it was the one that gave better results in terms of sensitivity. Furthermore, the fabrication process is well established providing good reproducibility. The patterning of the sensors was made via lift-off processes and photolithography techniques, with a serpentine geometry that gave the maximum length in a reduced area allowing the sensor to have more electrical resistance and consequently more sensitivity. The geometry of the RTD used consists of meander-shaped with 24 windings of a 200 nm platinum thin film (deposited by sputtering, as described in section 2.5.2) with a line width and spacing of 10 µm. These sensors were designed in a four-wire configuration, to ensure high accuracy and an output voltage directly proportional to the RTD resistance only.

In figure 10, it can be seen a wafer with various and in figure 11 sensors detailed photography of one fabricated sensor.

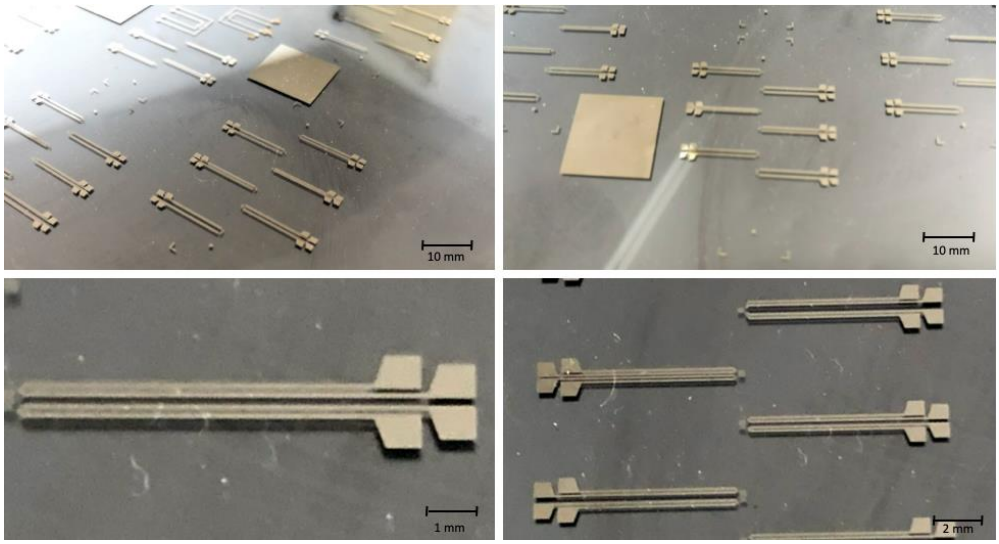

Figure 11 – Waffer with various aluminium sensors with the same geometry but different windings.

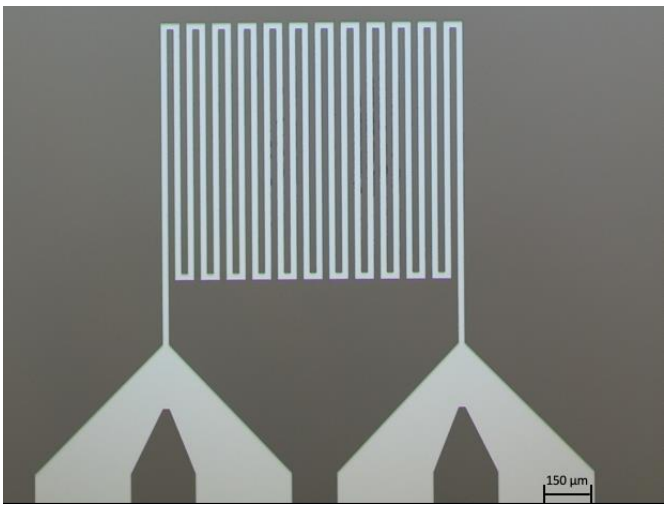

Figure 10 – Photography of the fabricated RTD.

These sensors operate with an excitation current and it was imperative to know how the sensor responds to every value of current to find the maximum value of current that the sensor can operate without self-heating. Previous works [59] showed that 100µA provides a negligible self-heating (0.008 °C), and thus, was selected for the following tests.

In the final part of the project, the developed system will be integrated into a microfluidic device with four temperature microsensors and a micro heating system. The main objective of this integrated system is to provide temperature optimal conditions for culture cells growth in OOC. The information collected by the sensors will be crucial to actuate the heating system and keep the environment at a temperature that the user wants.

3.1.3 Calibration techniques

To achieve high sensor effectiveness, several calibrations are required. Depending on the effectiveness required, calibration methods may be more expensive, i.e., the cost of calibration operation increases as sensor effectiveness increases. Typically, at the industry level where RTD is used, the temperature ranges used are small and this makes its calibration simpler [36]. The higher accuracy of a thermometer the more expensive the calibration technique is demanded. However, for some industrial-grade RTDs, it is possible to perform a simplified calibration technique because of the narrow temperature ranges they are used over. It is also essential that the calibration technique should draw less operator attention and optimize calibration time. In the publication of V. V. Gureyev *et al.* [36], a versatile semiautomatic method of calibrating industrial RTDs was presented with the use of the comparison method, comparing the response of the RTD to an industrial thermometer. There are two calibration methods:

Fixed point calibration

This calibration method is very precise, it can reach calibration close to 0.0001°C and consists of fixing the sensor to be calibrated inside a chamber with a limited number of fixed heating points at different temperatures but each maintains at its constant temperature during the process. These temperature values are known and selected through the International Temperature Scale of 1990(ITS-90) to select the minimum number of points. The points that are in ITS-90 have been documented and accepted by the global community [60].

Comparison method

In this calibration method, the sensor is compared to others that already have been calibrated and its response is compared within an environment and the temperature is known and controlled. There are several advantages to using this method in comparison to the fixed point method. Firstly, this method allows a variety of temperatures, rather than fixed temperatures and on a limited number. Another advantage is that these calibration systems are easy to use and allow calibration of multiple sensors at the same time and in an automated manner. This method is the most used to calibrate RTD's for industrial applications. However, it is necessary to pay maximum attention and ensure that the temperature of the thermostat is stable and uniform to avoid a lack of calibration effectiveness [36].

This method was used for the RTD calibration using a hotplate (Präzitherm type PZ28-2, 1100 W) with a resolution of 0.1°C which has a comercial sensor integrated which it was used for validation of the RTD sensor used.

4. SYSTEM DEVELOPMENT

After the methodology is defined, the electronic circuit for control and actuate the RTD will be developed. This system should be capable of measuring temperature changes, with a resolution of 0.1°C.

4.1 Control & actuation circuit

This is the most important part of the system since affect directly the performance of the sensors. A suitable current source and, amplification and filtering circuits are essential to ensure proper functioning. Everything has to be well chosen and implemented for low noise and accurate measurements.

4.1.1 Power source

The supply of the circuit was performed by batteries for assuring the independence of the power supply and portability. Two voltage regulators (L7805CV and L7905CV) were used to supply the circuit with 5V and -5V to power all the other components of the circuit- These supply values were chosen because the current source operates with 5V, and thus, to be easier to integrate and design of the circuit, all the other elements were also supplied with 5V and -5V.In figure 12, can be seen the designed power circuit. The capacitors must be all electrolytic and their values are according to the recommendations of the manufacturer of the regulators [40,41].

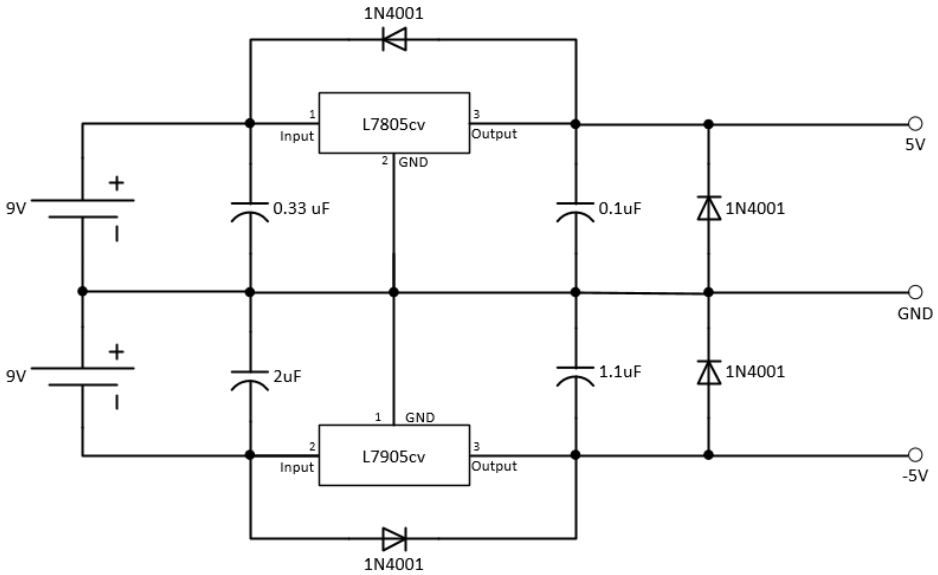

Figure 12 – Power source circuit with voltage regulation and protections.

4.1.2 Current source

The RTD needs an excitation current to operate and any fluctuation of the excitation current will originate a change in the electrical potential of the sensors, and consequently, will provide inaccurate temperature values. So, an adjustable current source (LM134 from Texas Instruments, Dallas, TX, USA) was used to provide a stable current of 100 µA. This device was chosen because it allows a current adjustment from 1 µA to 10 mA, with high accuracy and low noise.

In figure 13, it can be seen the implementation of the current source. This implementation is recommended by the manufacturer for this type of circuit that is temperature sensitive. The addition of a diode (1N457) and a second resistance (R2) cancels the temperature-dependent characteristic of the LM134 [63].

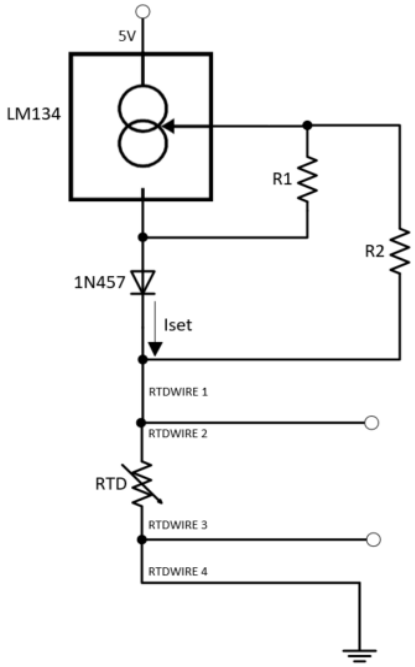

Figure 13 - Current source circuit to power the RTD.

To provide a stable current of 100 µA, the values of R1 and R2 must be calculated using the following equations:

$$Iset \approx \frac{0.134V}{R1} \quad (11)$$

$$R2 = 10R1 \quad (12)$$

Finally, with the value of 100 µA in *Iset*, it was obtained a value of 1.34kΩ to *R1* and 13.4 kΩ for *R2,* both resistance used are precision resistances with an 1% tolarance. The experimental value of the current measured with the implemented circuit can be seen in figure 14.

Figure 14 – Experimental excitation current using the implemented current source circuit.

4.1.3 Multiplexers

To select the sensor to read, it was chosen the multiplexer 4:1 (TMUX1104) since this component allows to read up to four sensors. This component is a low noise precision multiplexer that has a rail-to-rail logic, that enables operation in all ranges from GND to VDD, ultra-low leakage current, ultra-low charge injection and a fail-safe logic that allows the analogue pins to operate up to 5.5V regardless of the voltage in the supply pin [64]. In table 3, the truth table of the component is presented.

*X denotes don't care

Table 3 -Truth table of TMUX1104. Adapted from [64].

EN	A1	A0	Selected input to Drain(D) Pin
0	X^*	X^*	All channels are off
1	0	0	S1
1	0	1	S2
1	1	0	S3
1	1	1	S4

For the selection to be done successfully, the system must have two multiplexers, one for each group of wires (RTDXWIRE2 and RTDXWIRE3). The signal channels (A0 and A1) of the multiplexer will be connected and together connected to the two signal pins of the microcontroller, thus ensuring that the correct wires of the RTD are chosen simultaneously.

4.1.4 Amplification

For the amplification, it was chosen the high accuracy instrumentation amplifier AD620. Like is imperative through all the circuits is also a low noise component with an excellent DC performance, it has a gain range from 1 to 10 000 with high accuracy and low cost. It's ideal for this system as it has also a low power consumption [65]. AD620 has its gain programmed by a resistor (Rg) or other impedance. The equation to calculate the Rg is the following:

$$Rg = \frac{49{,}4k\Omega}{G - 1} \tag{13}$$

The output voltage of the temperature sensors used in this dissertation shows high linearity between temperature and electrical potential, ranging from 163.5 mV to 167.5 mV when the temperature is increased from 35 to 45°C. The ADC has a maximum input voltage stated at 3.3 V, so, a gain of 16 was defined, in this phase, allowing the output of the sensor to range from around 2.53 V to 2.6 V. Applying the formula, the value of the Rg is around 3.3kΩ.

Finally, the circuit responsible for the selection and amplification of the signal can be seen in figure 15

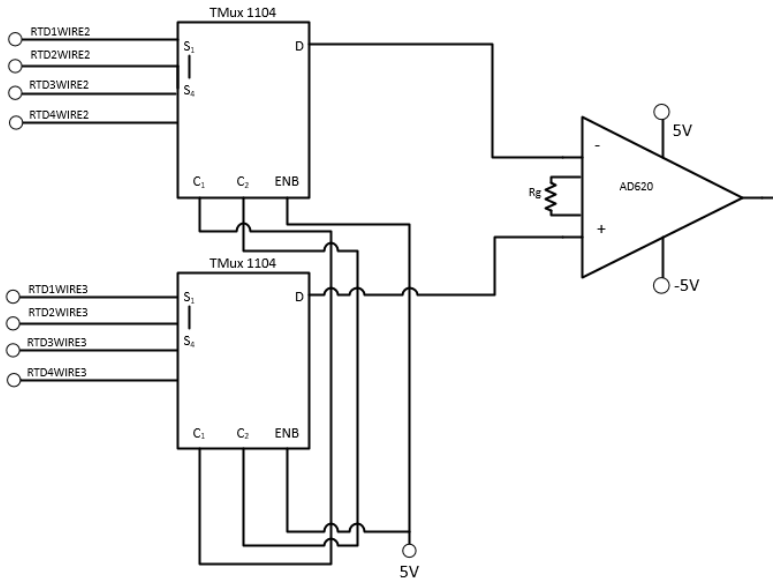

Figure 15 - Amplification circuit with the multiplexer.

4.1.5 Filtering

The amplification system is low noise but there was a need to attenuate the signal before it enters the ADC for better reading. It was implemented a first-order low pass filter with a cutting frequency of around 106 kHz. This frequency gives the better attenuation of the signal. With the value of the frequency, the values of the resistance and the capacitor that take part in the filter can be calculated with the following formula:

$$Fc = \frac{1}{2\pi RC} \tag{14}$$

where *Fc* is the cutting frequency (Hz), *R* the resistance (Ω) and *C* the value of the capacitor (*F)*. The value of the resistance calculated was 15 Ω and the capacitor was 100 nF.

In addition to that, an input filter was also implemented to prevent radiofrequency rectifications errors in instrumentation amplification. This type of error appears as a small dc voltage offset and normally occurs because all instrumentation amplifiers rectify small out of band signals. The input signal is limited by the filter according to the following two equations [65]:

$$FilterFreq_{DIFF} = \frac{1}{2\pi R(2C_d + C_c)} \tag{15}$$

$$FilterFreq_{CM} = \frac{1}{2\pi R C_c} \quad (16)$$

where, $C_d > 10C_c$.

The schematic of the circuit is shown in figure 16.

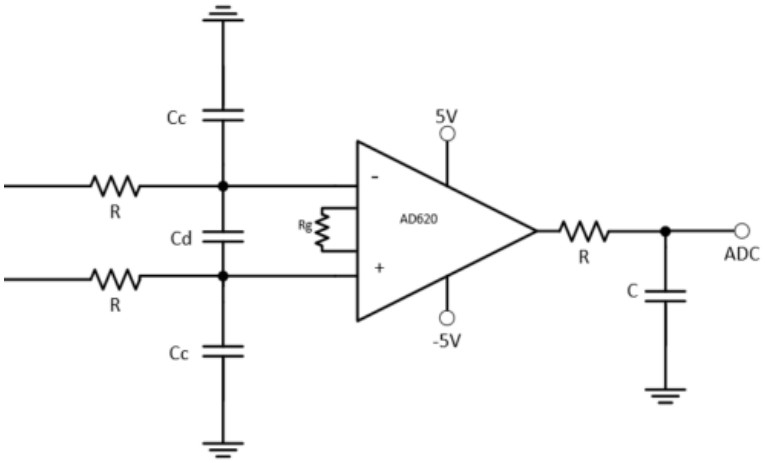

Figure 16 – Input filter that prevents RF amplification errors and low pass-filter.

The final version of the reading circuit can be seen in figure 17.

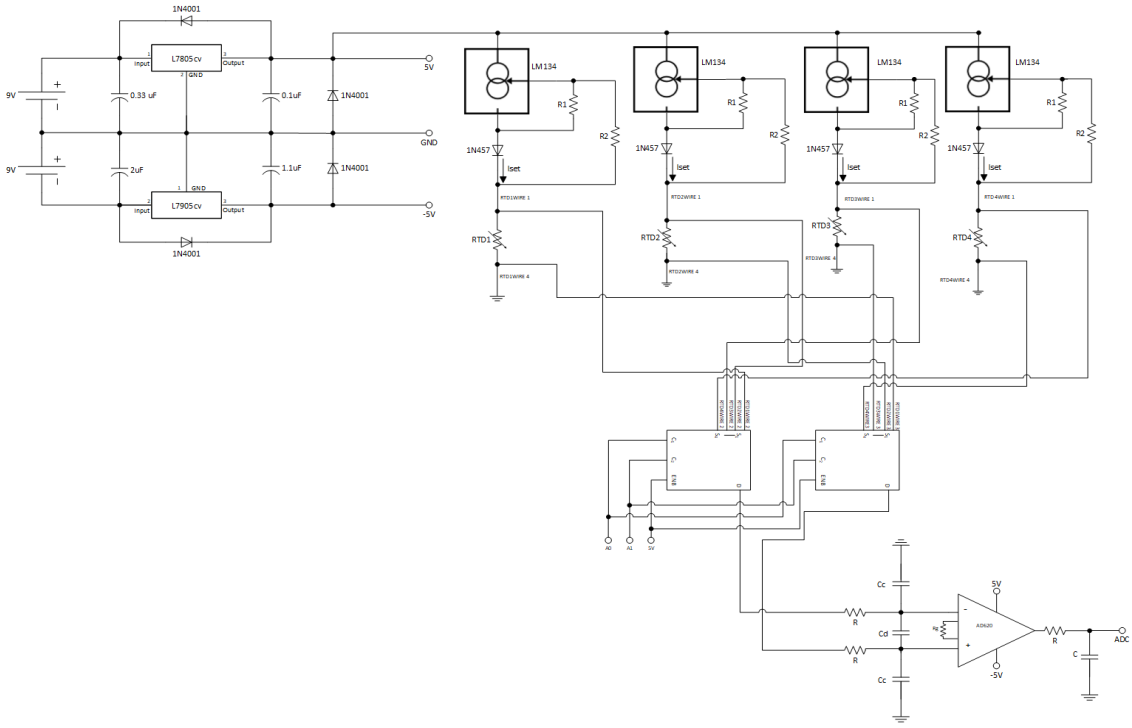

Figure 17 – Schematic representation of the final circuit.

4.1.6 PCB design

After validation of the system in a breadboard and later in a protoboard, the printed circuit board (PCB) was designed using the software “PADS Logic”. In the first instance, the component “Pads logic” was used to draw the schematic of the circuit (figure 18).

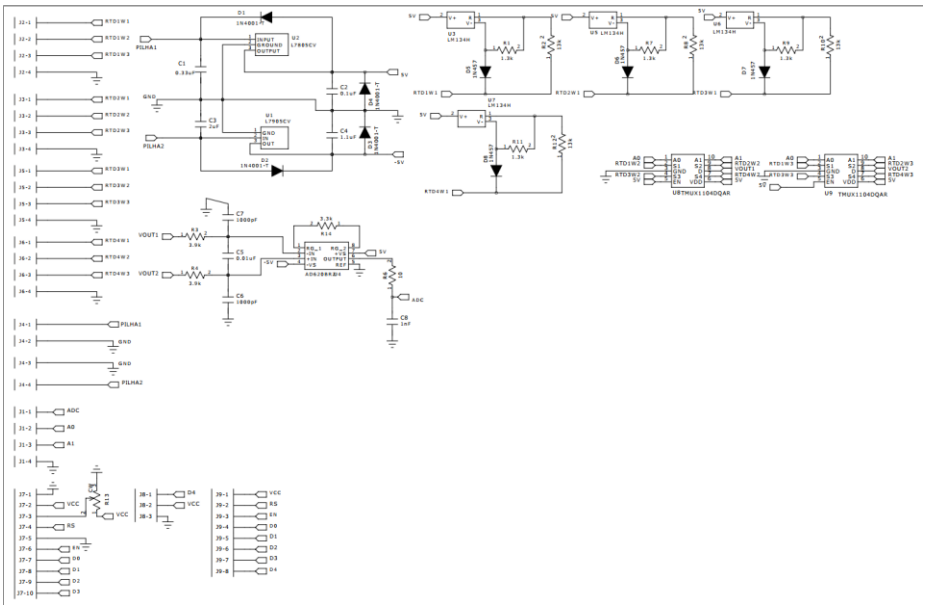

Figure 18 - Circuit schematic in PADS Logic.

Then, the software PADS Layout was used to transform the schematic in the final product before PCB manufacturing. This PCB comprises two layers because TMUX1104 and the AD620 are surface mounting devices (SMD) and in this way helps to integrate all components in a smaller PCB. In figure 19, are shown the top (figure 19 a) and bottom (figure 19 b) layers of the PCB. Both layers are connected to the ground.

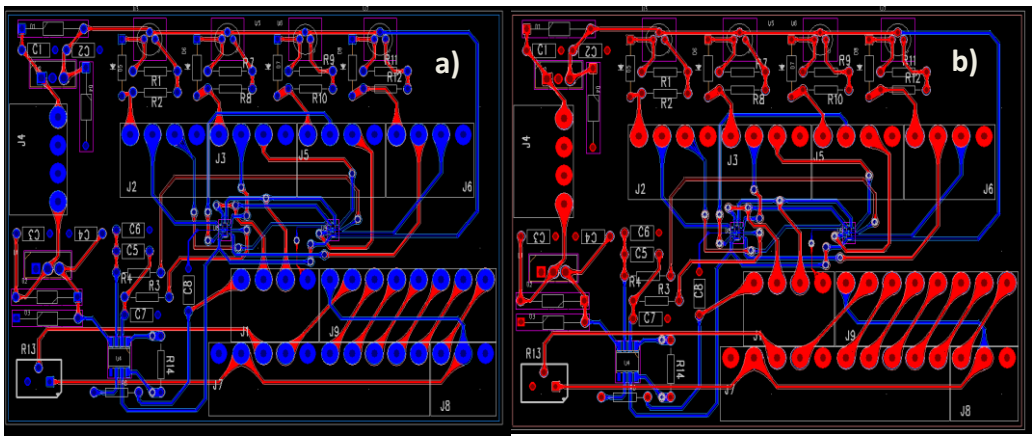

Figure 19 - Top and bottom view of the PCB design.

The fabricated PCB with the assembled components can be seen in figure 20.

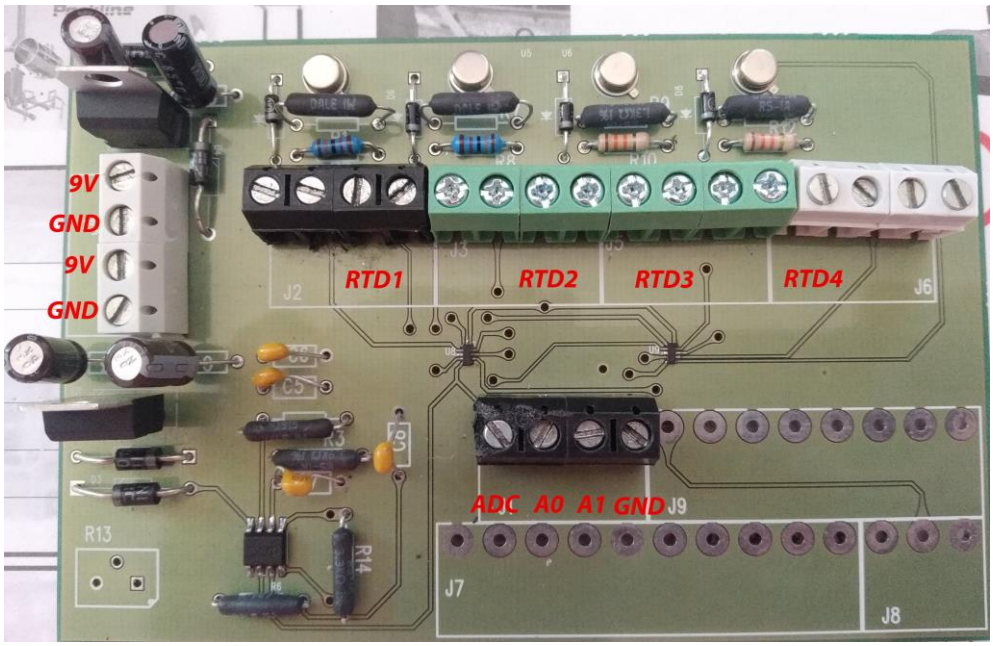

Figure 20 – Photo of the first prototype of the PCB assembled with all components.

4.2 Data acquisition

The data acquisition was performed with the development board STM32 Nucleo-F411RE (figure 21), which is responsible for the communication between the analogic part and the digital part through the ADC.

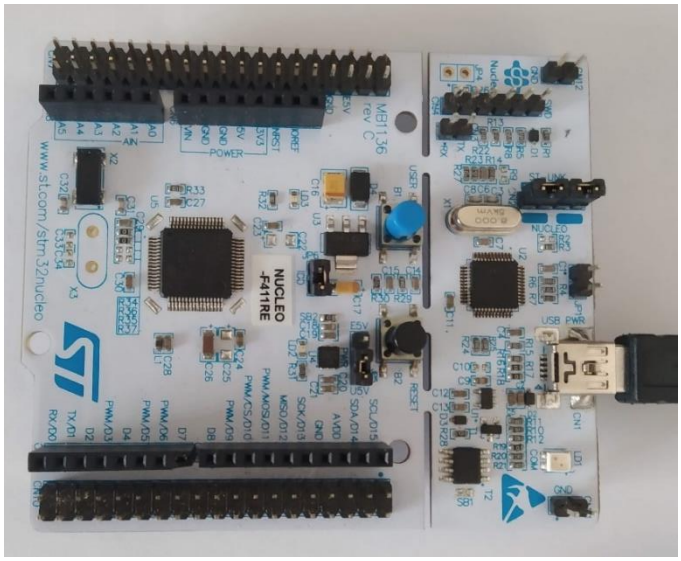

Figure 21 - Development board STM32 Nucleo-F411RE used to control and data acquisition.

The ADC has a resolution of 12 bits which gives a resolution of approximately 0.81mV. This value results from the following expression:

$$V = \frac{Maximum\ ADC\ voltage}{2^{bits\ of\ resolution}} = \frac{3.3V}{2^{12}} \approx 0.81mV \quad (17)$$

A sampling rate of 1kHz was chosen to allow the ADC to read every 1ms. The ADC module is operating on DMA mode, reading the values in the background, allowing the processor to do other operations in parallel. The values are summed up to a total of 250 values and the average is sent via UART with a baud rate of 11520 bps. This allows the values used in the conversion to be the most accurate possible without misrepresenting them.

The code implemented in the microcontroller for the reading and conversion of the voltage values is shown in figure 22.

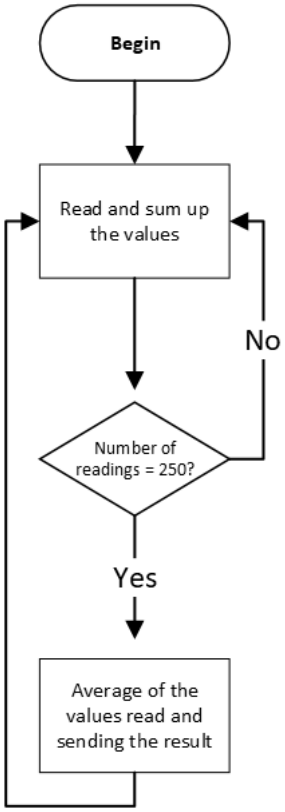

Figure 22 – Fluxogram of the reading and sending of the values.

In parallel, the microcontroller is always polling the UART port to check if any new command has been received from the graphical interface (figure 23).

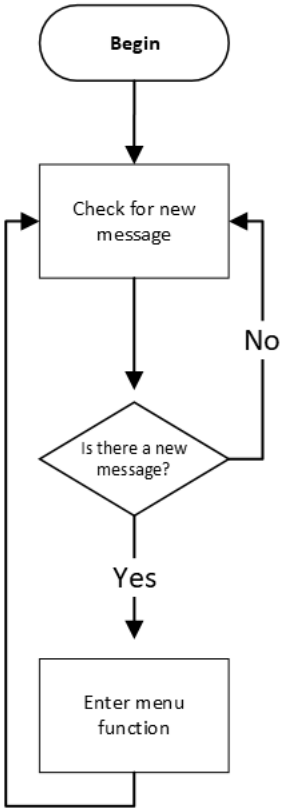

Figure 23 – The main loop, checking the UART port for new commands.

If a new command is received, it will be processed by a function “Menu” where the system decides what is to do according to the command (figure 24). It can connect/disconnect the board, start/stop the reading (figure 25), and change the RTD to be read (figure 26). All this information will be displayed in an LCD, which will have on the screen the state of the system and the RTD that is being read.

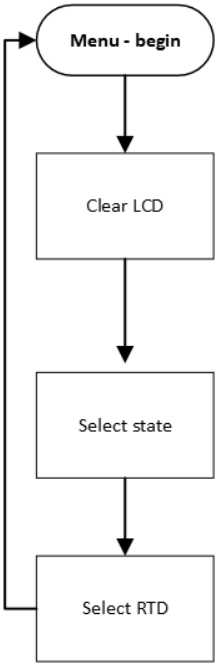

Figure 25 - Fluxogram of the menu function

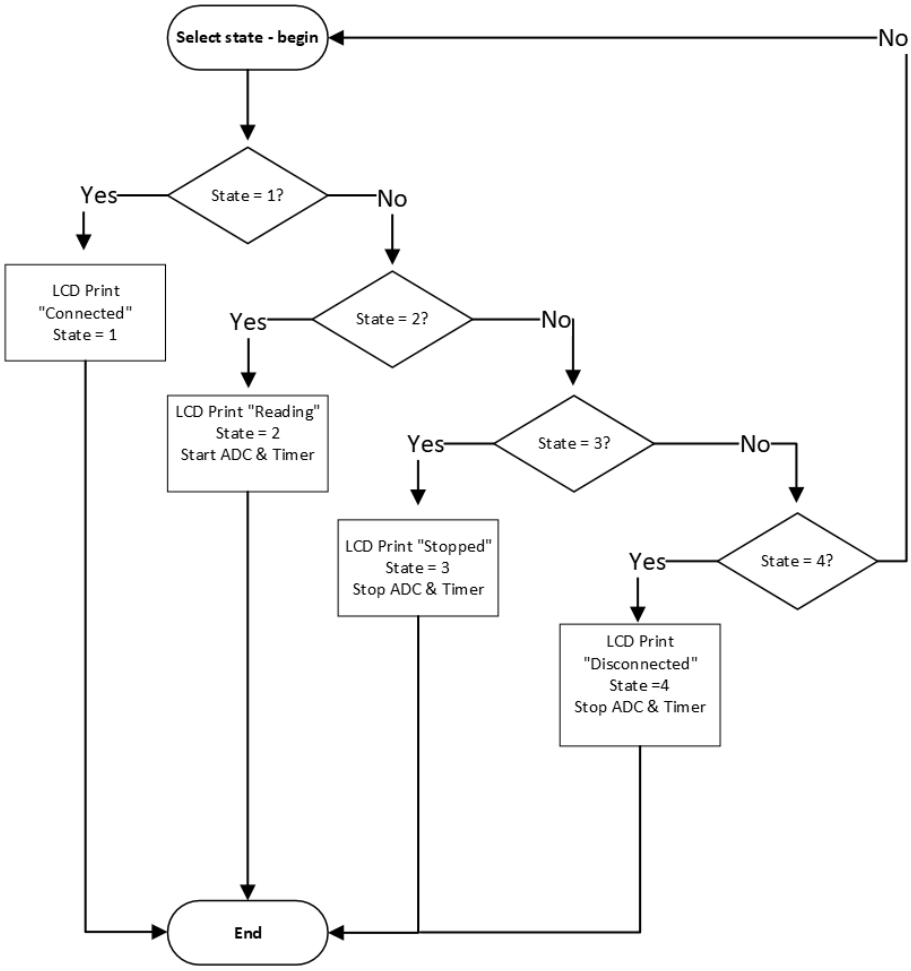

Figure 24 – Fluxogram of selection of state

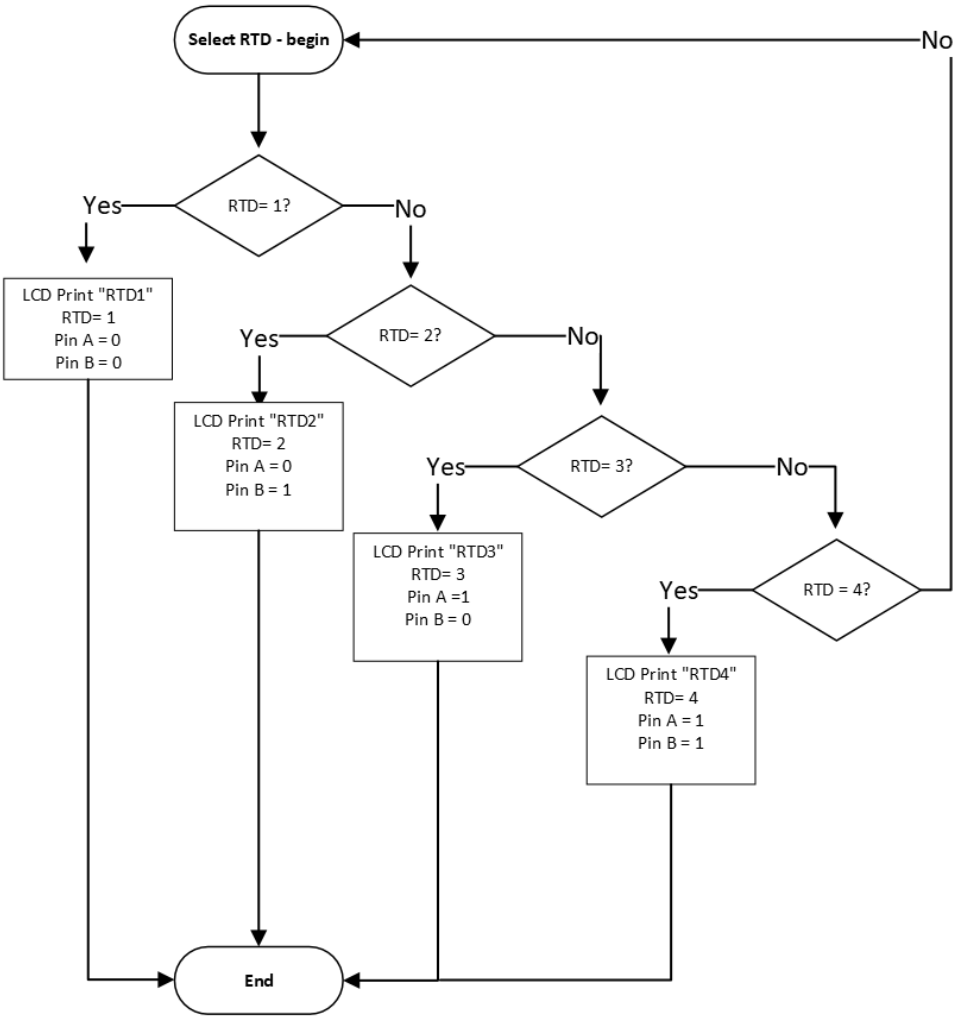

Figure 26 - Fluxogram of selection of the RTD.

4.3 Data visualizer

The data presentation comprises the graphical interface, where the results are converted by the microcontroller and displayed on a computer, and the LCD part where some information about the state of the system is displayed.

4.3.1 Graphical interface

The graphical interface is used to help the user to facilitate the data visualization from the several sensors. This interface can be resumed in a state machine presented in figure 27.

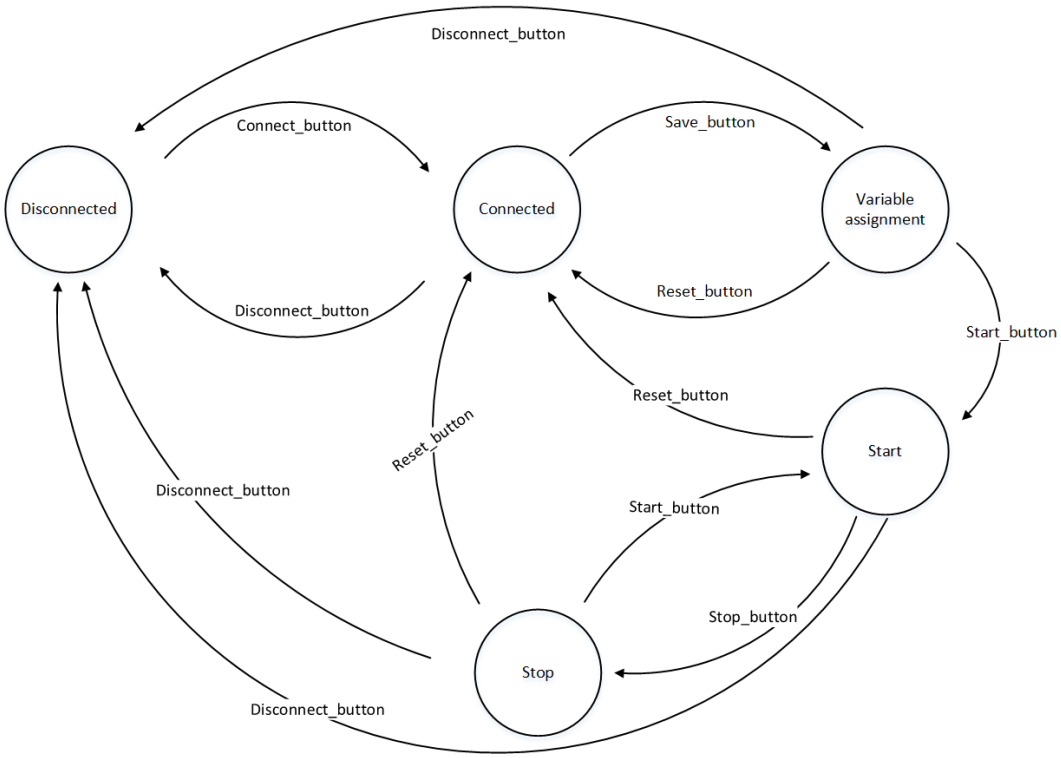

Figure 27 - State machine of the system.

As can be seen in figure 28 this graphical interface is very simple and user-friendly. Initially, it opens the first window for the definition of variables and RTD selection. It was also added some instructions to help the user understand how to use it. On the first window, the user connects the board, chooses the sensor that wants to read, inserts and saves the variables that will be used in the conversion and starts the reading. After this selection, a second window is open to show the temperature data that was converted and where the user can stop the reading and disconnect the board.

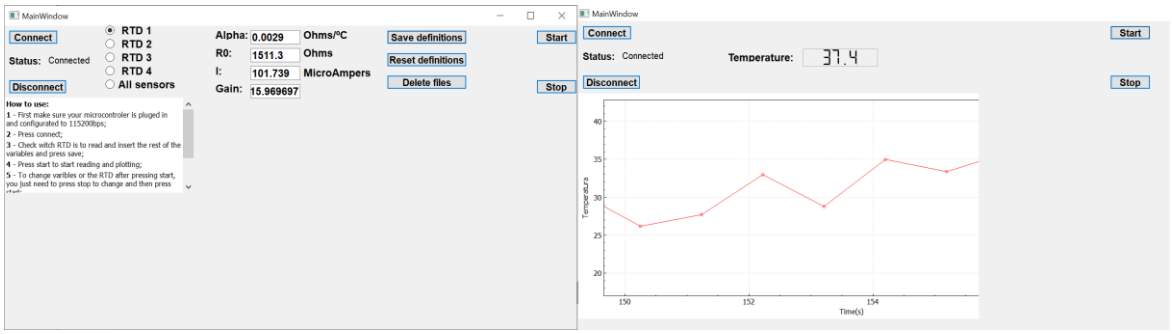

Figure 28 - Implemented graphical interface to choose and present the RTD response.

The system starts, as reset mode, in a state called “Disconnected” where the microcontroller is not reading values and is not connected to the computer The connection between the computer and the microcontroller is obtained by pressing the button “connect”. If the board is not connected correctly, an error message will appear and the system will stay in a state of disconnection. On other hand, if the connection is successful, a message will appear to inform that the connection was correctly performed (figure 29).

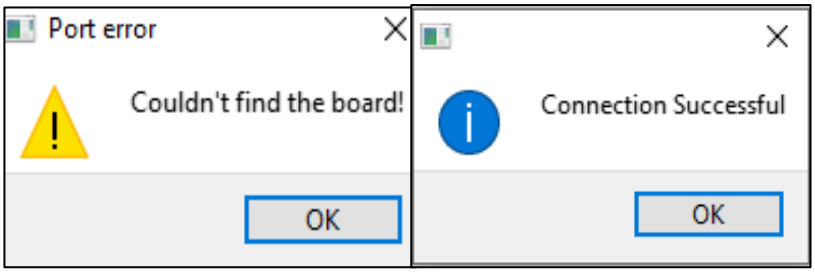

Figure 29 - Connection warnings.

Once the connection is made with success, the next step for the user is to choose the sensor to read and set the variables that will take part in the conversion of the voltage values to temperature. The user cannot start the reading without inserting values that are numeric and different from zero, as it shows an error message (figure 30 a). When the variables are all set, the user presses the save button to save the values of the variables and to send the number of the RTD that is going to be read by the microcontroller.

As the variables are successfully saved, a confirmation message will appear on the screen (figure 30 b). To reset the variables inserted, the user must press the reset button to erase the previous values and insert the new ones. Once the connection is made with success, the next step for the user is to choose the sensor to read and set the variables that will take part in the conversion of the voltage values to temperature. The user cannot start the reading without inserting values that are numeric and different from zero, as it shows an error message (figure 30 a). When the variables are all set, the user press the save button to save

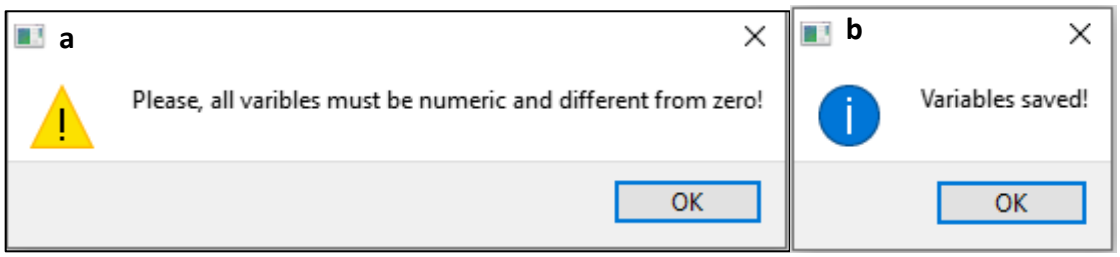

Figure 30 - Warnings related to variables insertion.

the values of the variables and to send the number of the RTD that is going to be read by the microcontroller.

Pressing start, the microcontroller initiates the reading and sends the values via UART. The program receives the voltage values which are converted to temperature and then are displayed in a graphical form and on a digital LCD. These converted values are also saved in a text file. Each sensor has a text file of voltage and temperature. The user can delete all the files by pressing the “delete files” button, otherwise, every reading is stored in the same text file of the previous reading. The user still has the possibility to see the temperature of the four sensors using the “All sensors” mode. This mode will change the sensor that is being read every 30 sec and save all the converted data in different files, one for each sensor.

Finally, the user has two options: 1) press stop and the system only stops reading and converting values or 2) disconnect all the system going back to the reset state of the system, by pressing the disconnect button.

4.3.2 Liquid Crystal Display (LCD)

As previously mentioned, the system has various states and allow select the RTD that is being read. This information will be displayed on an LCD. For this purpose, the LCD DFR0063 16x02 with communication via I2C protocol was used. The I2C protocol uses 2 wires, SCL (Serial Clock) and SDA (Serial Data) to communicate between the master, in this case, the microcontroller and the slave, in this case, the LCD. Firstly, the master sends a start condition followed by eight bits where seven are the slave address and the eighth bit is the mode that the communication is going to operate, 0 is to write and 1 to read from the slave. It waits for the acknowledge signal from the slave that the connection was made successfully. Then the master sends the data, one byte at a time and for each byte must wait for an acknowledged signal that the byte was well-received before sending the next byte of data. This operation

continues in this form until the master sends a stop condition to interrupt the communication. In figure 31, it can be seen the schematic of the communication.

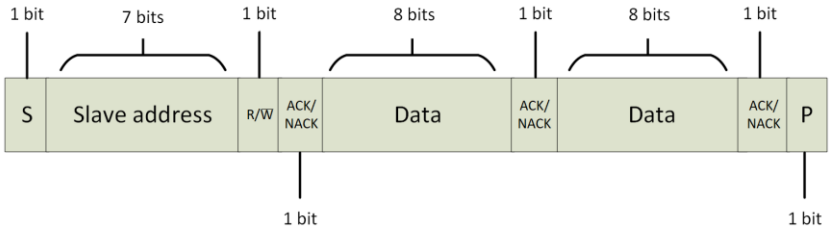

S = Start Condition;
R/$\overline{W}$ = 1 to read, 0 to write;
ACK/NACK = Acknowledged/Not-Acknowledged;
P = Stop condition.

Figure 31 - I2C communication protocol schematic.

In figure 32, it can be seen all the states that the LCD can show.

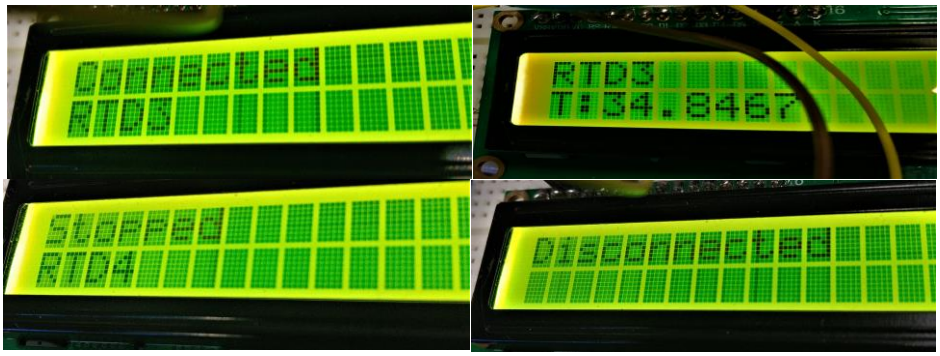

Figure 32 - LCD showing the four states of the system.

5. TESTS AND RESULTS

In this chapter, the experimental tests and consequent results of the project are presented and discussed. The development of the electronic circuits involved several test steps namely in 1) breadboard, 2) protoboard and 3) PCB testing. Improvements in the electronics circuits are also presented in this chapter.

5.1.1 Breadboard testing

Firstly, the circuit was implemented in the breadboard (Figure 33), without filter and with a gain of around 11 (as mentioned in section 4.1.4).

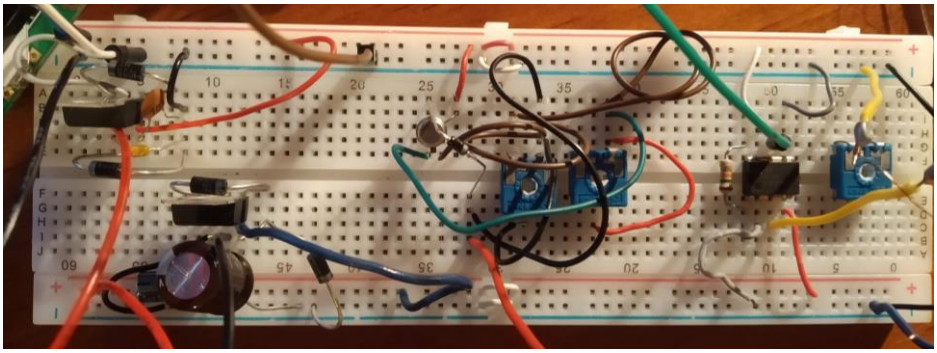

Figure 33 - Circuit implemented in the breadboard.

This testing was made to validate the sensor response using a hotplate with a resolution of 0.1°C to change the temperature. It was clear, as it can be seen in figure 34, that the sensor was responding as expected, its output voltage increased with a sensitivity of 0.73 mV/°C. However, the system still had some perturbation derivated from noise and present a poor resolution.

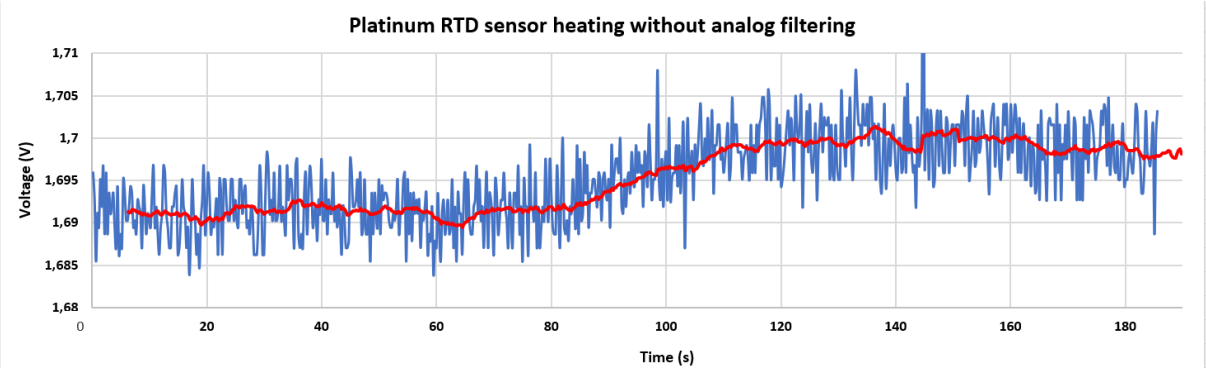

Figure 34 - Microsensor response with implemented electronics to temperature variation from 35 to 45 °C without filtering.

After this, a filter with a cutting frequency of 106 kHz was implemented to permit the reading of low-frequency signals and attenuates frequencies higher than the cutting frequency. As can be seen in figure 35, the noise was substantially reduced, but the

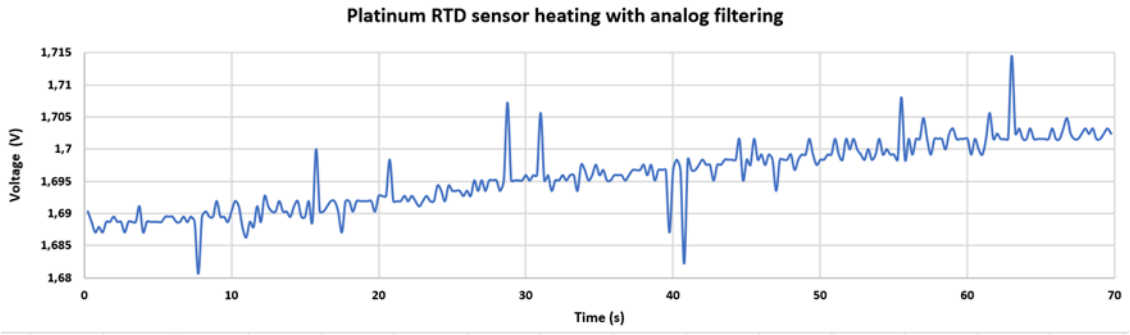

Figure 35 - Output voltage of the sensor with filtering when the temperature is increased from 35 °C to 45 °C.

amplification circuit still has poor resolution since from 35°C to 45°C the output voltage only changes around 10mV. Since it is intended to read the sensor's response with the STM, the output range must change significantly. Furthermore, the output voltage still has a significant level of noise, especially when is intended to read with a resolution of 0.1°C.

5.1.2 Protoboard testing

The next step was the implementation of the circuit in a Protoboard which can be seen in figure 36. This circuit helped reduce the noise from the breadboard tracks and to validate these changes before implementing the PCB. This circuit didn't have yet the AD620 and the TMUX1104 because as at this stage the only objective was to validate the response of the sensor. This circuit was used an instrumentation amplifier INA126 to validate the amplification system.

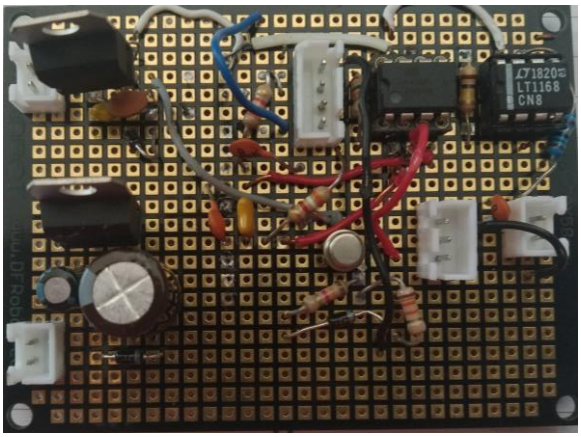

Figure 36 - Circuit implemented in Protoboard.

Also, the reading frequency of the ADC was increased to 1kHz, which is equivalent to reading values each 1 ms. In figure 37, it can be seen the output voltage of the circuit in the protoboard when the temperature was increased from 35°C to 45°C.

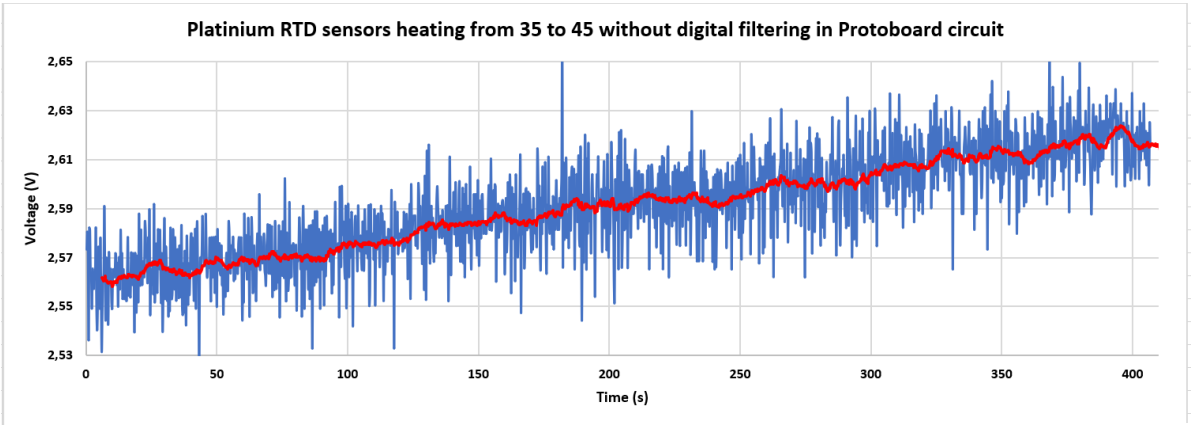

Figure 37 - Results with ProtoBoard circuit. Heating from 35°C to 45°C.

High levels of fluctuations and noise are verified in the output voltage when this assemble was used. The ProtoBoard still produces noise from the connections between the components and, theoretically, the INA126 is not the ideal component compared to the AD620, as it produces more noise comparing both characteristics [59,60]. Also, a digital technique of summing up the values of 250 readings and taking the average number of that sum was implemented to remove output voltage picks of the sensor response (figure 38). In this graph, there are two cycles: 1) the blue line represents an increase of temperature from 35 to 45°C and 2) the orange line decrease temperature from 45 to 35°C. It can be noted that the voltage picks were softened as expected but there is still some noise and instability that comes from the ProtoBoard circuit. A sensitivity of 3.37mV/°C was obtained with this approach.

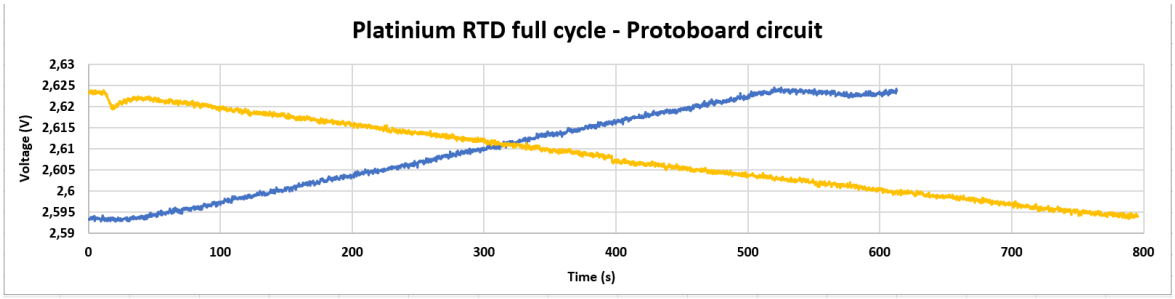

Figure 38 - Results of a full cycle of heating and cooling of the system from 35°C to 45°C in Protoboard.

5.1.3 PCB testing

After validation of the entire circuit with breadboard and protoboard, the PCB was designed and manufactured with all the necessary circuits. After manufacture, the experimental setup shown in figure 39 was used to characterize the response of the sensors using the PCB circuit.

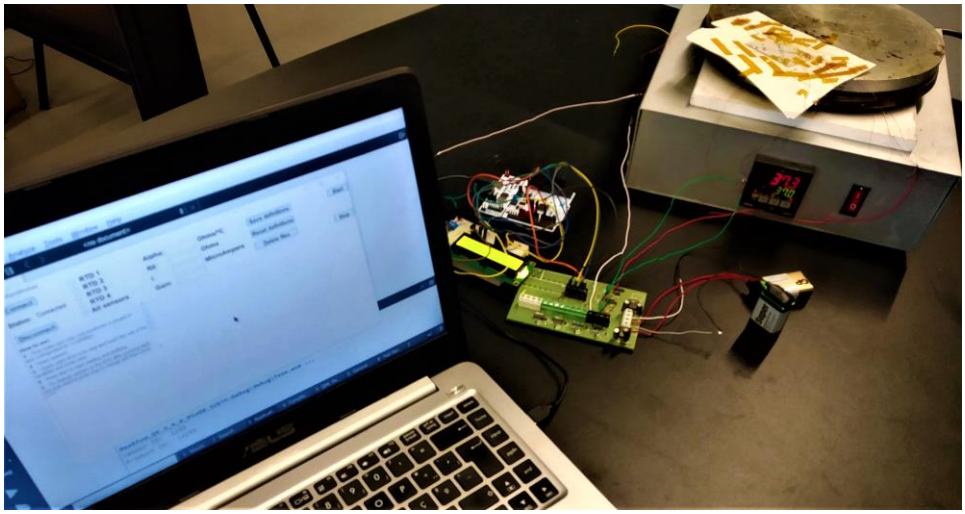

Figure 39 - Experimental setup used for the temperature microsensor characterization using the implemented PCB.

Several heating and cooling cycles between 35 and 45°C were applied to validate the PCB circuit. Figure 40 shows one of these tests with stabilization at 40°C. The response was similar to previous tests, however, it is verified greater stability of the response with lower fluctuations and noise. A sensitivity of 7.61 mV/°C was obtained with this approach.

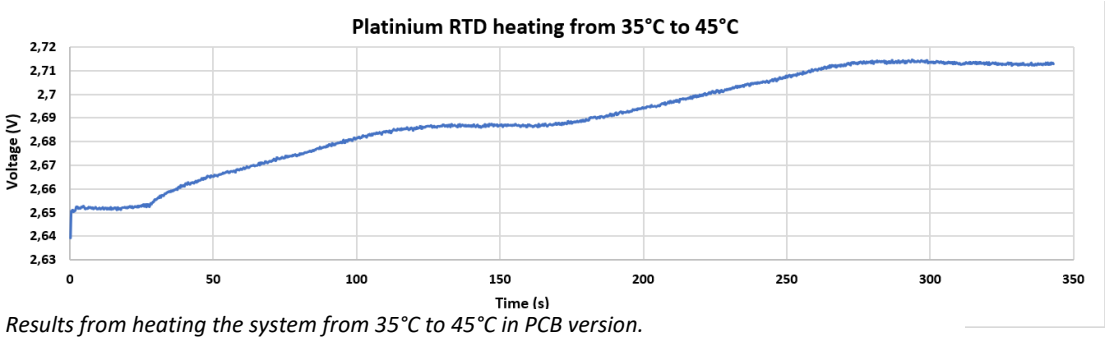

Figure 40 - Results from heating the system from 35°C to 45°C in PCB version.

From the characterization of the sensor response, it was necessary to implement a step of conversion of the output voltage of the system into temperature values. For that was used the equations mentioned in chapter 3, in subsection 3.1.1 This characterization was made using the comparison method, comparing the values of the RTD against the sensor of the hotplate.

In the developed software it is possible to define specific variables for each of the sensors to be measured, i.e., gain, R0 and α. The R0 and α values were obtained from the measurement of the electrical resistance value of the RTD using a digital multimeter (Agilent 34410A 61/2). The measured resistance values are shown in the graph in figure 41. From these values, it was possible to define the calibration line and calculate the R0 and R100, and consequently the α.

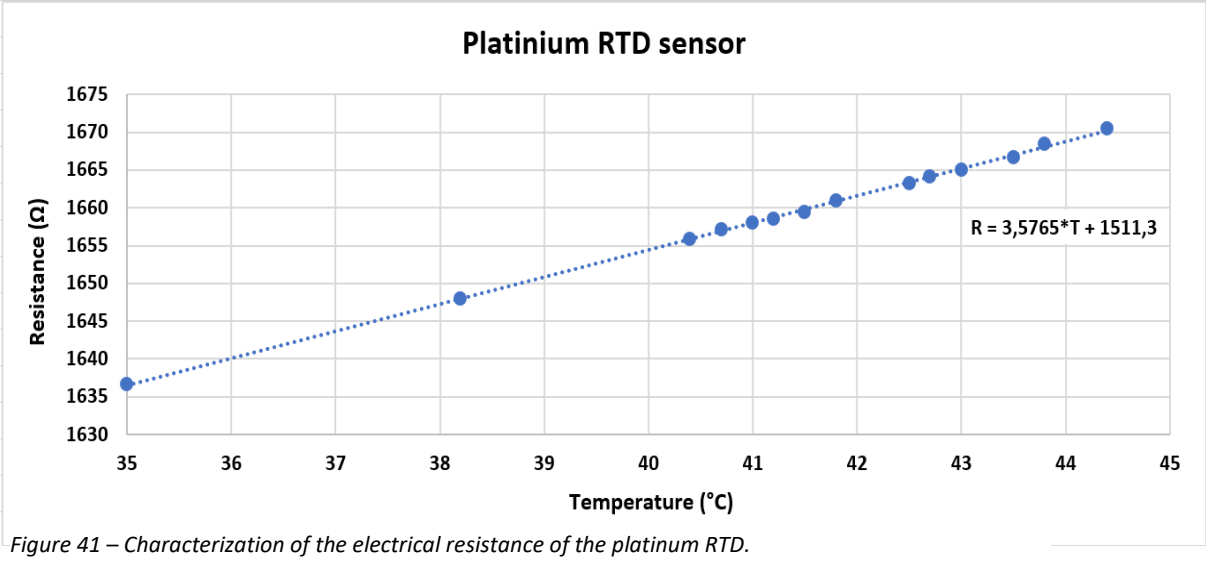

Figure 41 – Characterization of the electrical resistance of the platinum RTD.

So, the straight equation is the following:

$$R = 3{,}5765 * T + 1511{,}3 \tag{18}$$

and this gave a value of $R0$ of 1511,3 Ω and also a value of $R100$ of 1869,09 Ω. With these two values, it was possible also calculate the practical value of the temperature coefficient of resistivity (α) using the following equation:

$$\alpha = \frac{R100 - R0}{R0 * \Delta T} \tag{19}$$

where R100 and R0 are the values of resistance and ΔT is the difference of temperature, in this case, 100°C. The practical value of the coefficient for this sensor was 0.002367432 Ω / Ω /°C. This difference in the value can be explained by the fact that these sensors are fabricated in thin film and the theoretical value of the platinum was defined for the bulk material.

In order to assess if the sensors are able to measure temperature changes of 0.1°C, was used a hotplate to apply a heating cycle between 37.5 ℃ to 38.9 ℃ with an increment of 0.1°C. In figure 42 are showed the converted temperature values of these tests.

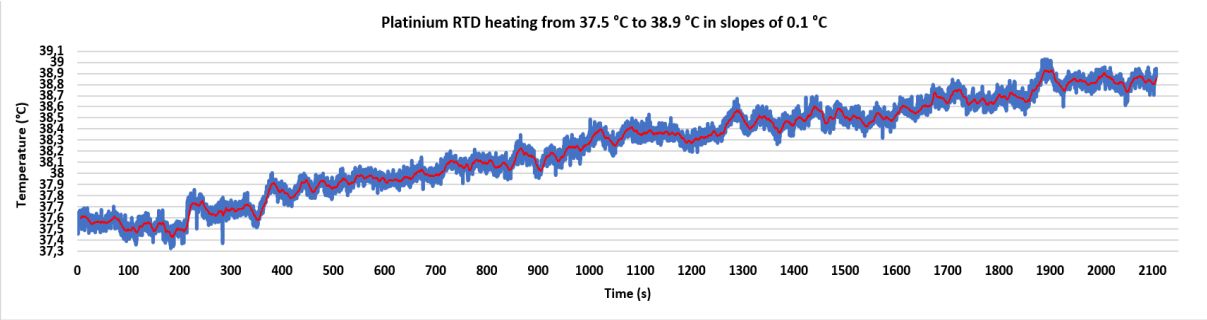

Figure 42 - Results from the heating test with increments of 0.1°C from 37.5°C to 38.9°C.

With these results, it can be seen that the sensor is responding properly to the temperature increments, despite some difficulty to keep a constant temperature in each step due to the instability of the hotplate (lack of isolation and heating losses). However, even if is possible to see the variations of 0.1°C, the output voltage is still low for the resolution wanted.

5.1.4 Improvements of the circuit

With the objective of increasing the resolution of the system, was implemented a new approach with two stages of amplification using the AD620. On this approach, was given special attention to the reference voltage of both AD620 to optimize the output to range between 0 and 3.3V (voltage values measured by ADC) The first stage of amplification has an RG = 1kΩ, which gives a gain of around 50.4 and on the second stage, the RG is 7.8kΩ which gives a gain of around 7.33. The combination of these two gains provides a total gain of around 369.6.

To assure that the output ranges between 0 and 3.3v for the desired temperature range (35°C to 45°C) the reference of the first stage was connected to -10V to allow the system to have a more amplification range. With the output of the first stage connected to the positive entrance of the second stage, the negative entrance can match the output value of the temperature that is wanted to be the first value of the temperature reading.

In this case, 23°C was chosen to be the initial value. The voltage value corresponding to this temperature is connected to the negative entrance and the amplifier will subtract both

entrances making his output 0V at 23°C, and from there, all the values are positive and increase with the increase of temperature.

The low-pass filter was maintained the same and the new amplification circuit is shown in figure 43.

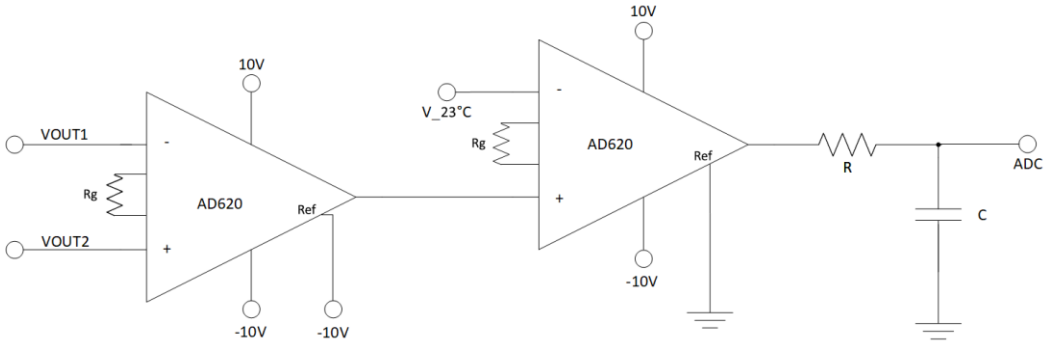

Figure 43 - New amplification circuit with two floors of amplification.

Using this new amplification circuit, the response of the sensor was characterized again using the comparative method against the sensor of the hotplate in order to predict which output value of the new circuit gives to every temperature. In figure 44 it can be seen the graph made with some points of temperature and its practical voltage values.

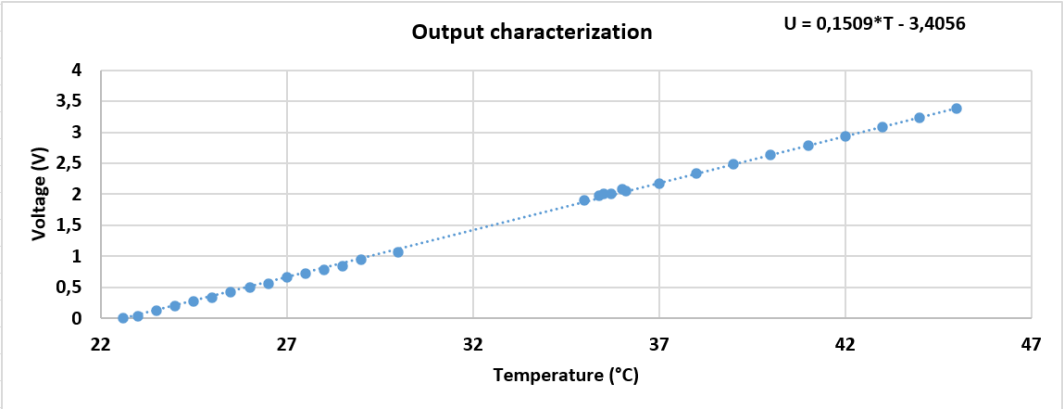

Figure 44 – Output voltage of the RTD using the improved amplification circuit.

The following table presents the experimental values of voltage measured for each value of temperature in the interval of 35°C and 45°C for this new amplification circuit.

Table 4 - Practical output values of the system for each temperature in the range of 35°C to 45°C.

Temperature (°C)	Output voltage (V)
35	1.8759
36	2.0268
37	2.1777
38	2.3286
39	2.4795
40	2.6304
41	2.7813
42	2.9322
43	3.0831
44	3.234
45	3.3849

The experimental setup used to validate the improved circuit is shown in figure 45. An external voltage source was used to power the excitation and the amplification circuits.

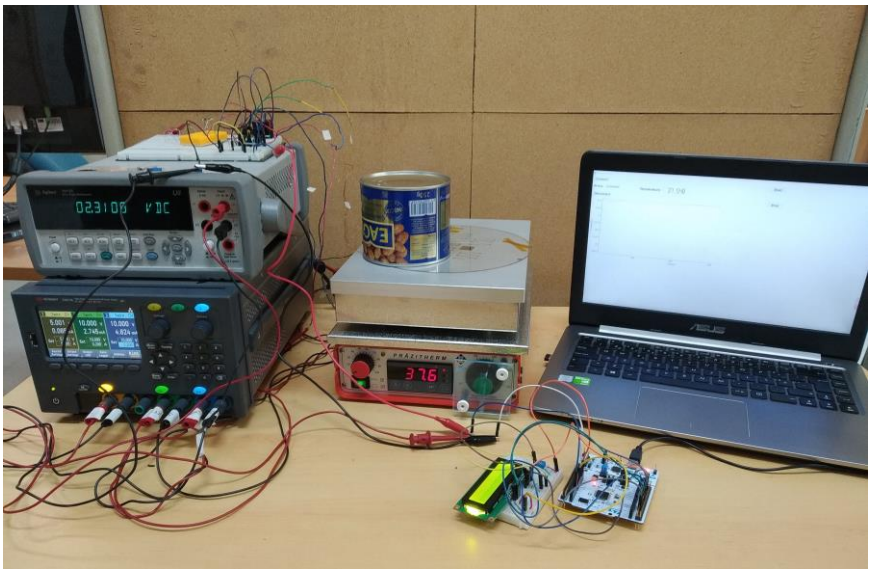

Figure 45 - Experimental setup used for testing the improved circuit.

The value of 45°C is at the limit of 3.3V which means that the value at the output of the second floor instead of being 0V at 23°C could be passed to 24°C allowing the system to reach 45°C without reaching the limit of the voltage of the ADC. However, it is possible to say that the improvements increase the sensitivity to 0.1509V/°C.

Finally, the system was tested to validate the improved circuit together with the graphical component and show that the resolution of 0.1°C was achieved. In figure 46 it is possible to verify the acquisition of various temperature values when the temperature was increased from 39.7 to 40.3°C, which prove the resolution of 0.1°C.

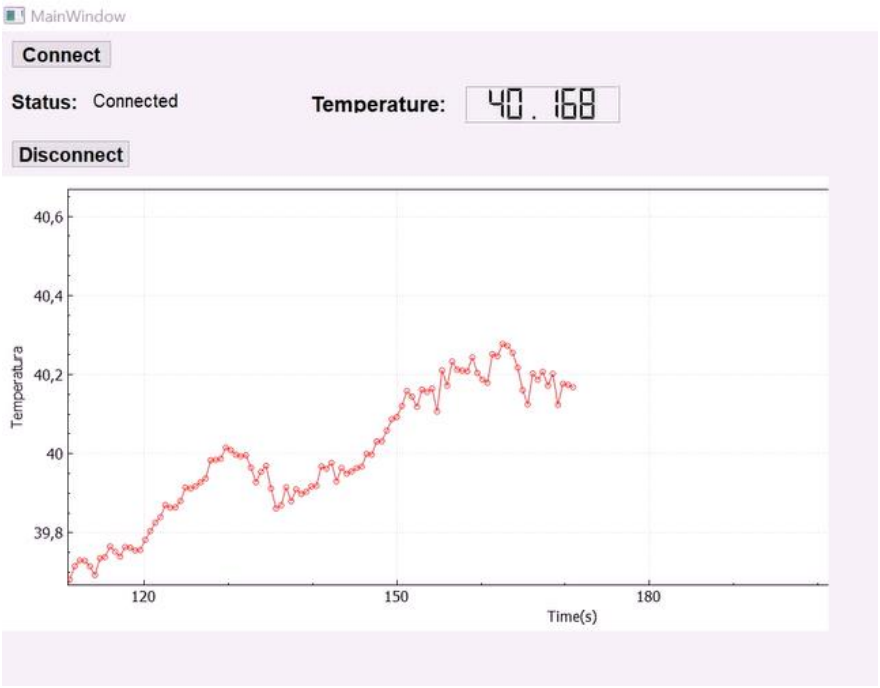

Figure 46 – Graphical interface showing the temperature value when a heating cycle between 39.7 and 40.3°C was applied.

6. CONCLUSIONS AND FUTURE WORK

In this chapter, it will be presented the main conclusions of this work and some suggestions that could contribute to future developments of this project.

6.1 Conclusion

In this dissertation, it was proposed the development of an electronic system to control and read miniaturized temperature sensors to be integrated with an organ-on-a-chip device. Throughout this document presented all the state of art necessary to this project, its implementation and results. This work was divided into two components, analog and digital electronics.

For the analog component, the objective was to develop a system that could read multiple sensors, while aiming for a low noise circuit and a reading resolution of 0.1°C. During the development of this system and with the achieved results, the system was optimized to reach as close as possible the predefined objective.

After the analysis of the previous works with these sensors, the current value of 100 µA from the current source circuit to power the sensor, provided by the circuit described in section 4.1.2, was proven to be the best value for preventing the sensor from self-heating.

In the final circuit, the majority of the components worked as was supposed to. Firstly, the power source and the components used in the circuit fulfilled the goal of powering all the circuit. The LM134 was also proven to be a good choice for the current source as it is a low noise component and with a precision value of current. The chosen amplifier proved to be suitable for this work because of its margin of gain and also due to being a low noise component. Although the amplifier's gain was enough for the amplification purpose, it was concluded that only one stage of amplification was not enough to get the resolution that was needed because of restrictions from the ADC of 3.3V as the maximum of tension that it can read. This required changes in the amplification circuit, after being assembled to the PCB, thus these hardware changes were implemented in a breadboard and their experimental tests confirmed the low noise required, as the output values were very stable.

In the digital component, the STM32F411RE microcontroller fulfilled its purpose with an ADC with good resolution, providing a maximum resolution of 0,81 mV which is revealed

to be enough to capture the variations of 0.1°C as these temperature variations were around 15 mV.

A clear and simple user-interface was developed containing the features that were proposed. The user is capable of selecting the sensor to be read and it can access easily the results that are being converted in real-time through the text files that are being created as the temperature values are converted. Also, the LCD was working as supposed, showing all the states of the system and its temperature.

6.2 Future work

In future work, although the system is working as it is proposed, there are some improvements that can help to have even more resolution and take this system to another level, if that is required for the future.

In the analog component of the system, the main change that can be made is to implement this new version of the circuit in PCB with all the components being SMD, as this will reduce the noise that the system could still have and significantly will reduce the size of the circuit.

One other change that could be made is the value in the negative input of the second stage of amplification to the value of output voltage of 30 °C, making that temperature the starting point of conversion (0 V) and with that, the gain of the second stage could be higher, allowing the system to have an even higher resolution as this change would help to get more advantage of the range of operation of the ADC.

On a digital level, the microcontroller could be changed for another one with higher ADC resolution and have more input channels as this will allow reading the output values of more than one sensor at a time.

In the graphical component, some features could be added:

- The capability of loading a text file with the information of the sensor that will be read instead of, in each reading, the user inserts the variables for the conversion of temperature;
- The graph could be displayed in two windows: 1) As it is, in real-time; 2) static printing the temperature in an interval of time defined by the user, allowing to

see all the evolution of the temperature throughout all the reading with the capability of saving that same graph in an image;

- Having a window for each sensor;
- A protection system could also be implemented, warning the user of possible temperature values outside the limits that the system is supposed to operate, turning on warning signals.

Furthermore, it is important, in the future, to evaluate the performance of the system integrated with a microfluidic channel that will be used in an OOC application. A prototype developed already by the CMEMS shown in figure 47 illustrates how the sensors would be displayed in the microfluidic channel.

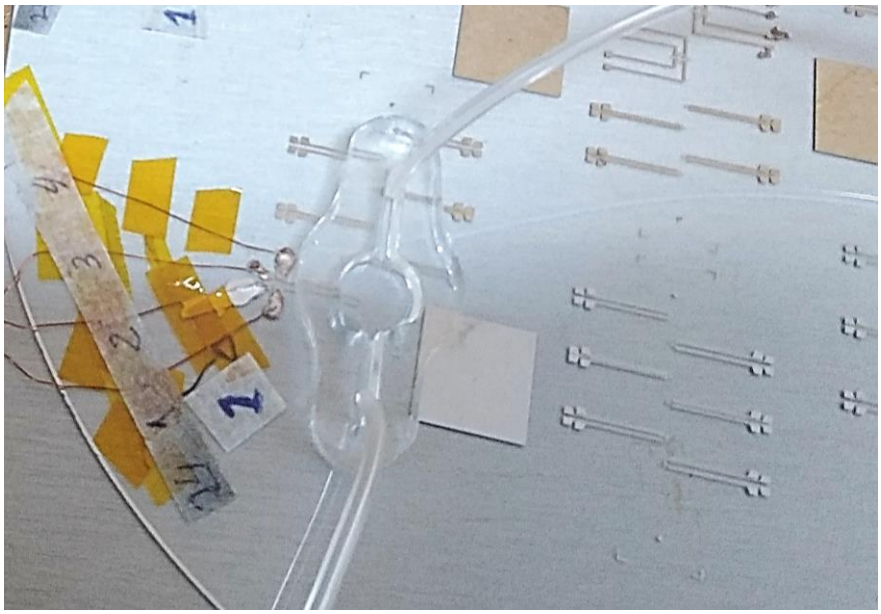

Figure 47 - Microfluidic channel prototype integrated with the platinum RTD sensors.

BIBLIOGRAPHY

[1] J. E. Sosa-Hernández *et al.*, "Organs-on-a-Chip Module: A Review from the Development and Applications Perspective," *Micromachines*, vol. 9, no. 10, 2018, doi: 10.3390/mi9100536.

[2] H. Mauriac, C. Pannetier, and G. V. Casquillas, "Organs on chip review," *Elveflow*, Dec. 2020, Accessed: Dec. 19, 2021. [Online]. Available: https://www.elveflow.com/microfluidic-reviews/organs-on-chip-3d-cell-culture/organs-chip-review/.

[3] Q. Wu *et al.*, "Organ-on-a-chip: Recent breakthroughs and future prospects," *Biomed. Eng. Online*, vol. 19, no. 1, pp. 1–19, 2020, doi: 10.1186/s12938-020-0752-0.

[4] B. A. McKenzie and W. H. Grover, "A microfluidic thermometer: Precise temperature measurements in microliter-and nanoliter-scale volumes," *PLoS One*, vol. 12, no. 12, pp. 1–14, 2017, doi: 10.1371/journal.pone.0189430.

[5] J. Kim, J. Kim, Y. Shin, and Y. Yoon, "A Study on the Fabrication of an RTD (Resistance Temperature Detector) by Using Pt Thin Film," *Korean J. Chem. Eng.*, vol. 18, no. 1, pp. 61–66, 2001, doi: 10.1007/BF02707199.

[6] J. Wu, "A Basic Guide to RTD Measurements," *Texas Instruments Inc.*, no. June, pp. 1–42, 2018.

[7] O. Cann, "These are the top 10 emerging technologies of 2016 | World Economic Forum," *World Econ. Forum*, 2016, Accessed: Nov. 26, 2020. [Online]. Available: https://www.weforum.org/agenda/2016/06/top-10-emerging-technologies-2016/.

[8] G. M. Whitesides, "The origins and the future of microfluidics," *Nature*, vol. 442, no. 7101, pp. 368–373, 2006, doi: 10.1038/nature05058.

[9] J. Chen, D. Chen, Y. Xie, T. Yuan, and X. Chen, "Progress of microfluidics for biology and medicine," *Nano-Micro Lett.*, vol. 5, no. 1, pp. 66–80, 2013, doi: 10.3786/nml.v5i1.p66-80.

[10] T. Chen *et al.*, "A drug-compatible and temperature- controlled microfluidic device for live-cell imaging," 2016.

[11] M. Gonidec and J. Puigmartí-Luis, "Continuous-versus segmented-flow microfluidic synthesis in materials science," *Crystals*, vol. 9, no. 1, 2019, doi: 10.3390/cryst9010012.

[12] B. K. Gale *et al.*, "Low-Cost MEMS Technologies," *Ref. Modul. Mater. Sci. Mater. Eng.*, 2016, doi: 10.1016/B978-0-12-803581-8.00530-0.

[13] W. Quispe-Tintaya, "乳鼠心肌提取 HHS Public Access," *Physiol. Behav.*, vol. 176, no. 3, pp. 139–148, 2017, doi: 10.1039/c6lc00163g.The.

[14] E. Roy, J.-C. Galas, and T. Veres, "Thermoplastic elastomers for microfluidics: towards a high-throughput fabrication method of multilayered microfluidic devices.," *Lab Chip*, vol. 11, no. 18, pp. 3193–3196, Sep. 2011, doi: 10.1039/c1lc20251k.

[15] X. Li, D. R. Ballerini, and W. Shen, "A perspective on paper-based microfluidics: Current status and future trends," *Biomicrofluidics*, vol. 6, no. 1, 2012, doi: 10.1063/1.3687398.

[16] Y. Cong *et al.*, "Drug toxicity evaluation based on organ-on-a-chip technology: A review," *Micromachines*, vol. 11, no. 4, pp. 1–24, 2020, doi: 10.3390/MI11040381.

[17] T. Kilic, F. Navaee, F. Stradolini, P. Renaud, and S. Carrara, "Organs-on-chip monitoring: sensors and other strategies," *Microphysiological Syst.*, vol. 1, no. 2, pp. 1–1, 2018, doi: 10.21037/mps.2018.01.01.

[18] E. Verpoorte *et al.*, "HOW MICROTECHNOLOGIES ENABLE ORGANS-ON-A-CHIP Pharmaceutical Analysis , 2 Pharmacokinetics , Toxicology & Targeting , Groningen Research Institute of Pharmacy , University of Groningen , Groningen , The Netherlands Endothelial Biomedicine and Vascular Dru," pp. 224–227, 2015.

[19] B. Zhang, A. Korolj, B. F. L. Lai, and M. Radisic, "Advances in organ-on-a-chip engineering," *Nat. Rev. Mater.*, vol. 3, no. 8, pp. 257–278, 2018, doi: 10.1038/s41578-018-0034-7.

[20] B. J. Kane, M. J. Zinner, M. L. Yarmush, and M. Toner, "Liver-specific functional studies in a microfluidic array of primary mammalian hepatocytes," *Anal. Chem.*, vol. 78, no. 13, pp. 4291–4298, 2006, doi: 10.1021/ac051856v.

[21] D. Huh, B. Matthews, A. Mammoto, M. Montoya-Zavala, H. Hsin, and D. Ingber, "Reconstituting Organ-Level Lung Functions on a Chip," vol. 328, 2010, [Online]. Available: https://science.sciencemag.org/content/328/5986/1662.

[22] K.-J. Jang and K.-Y. Suh, "Miniaturisation for chemistry, physics, biology, & bioengineering A multi-layer microfluidic device for efficient culture and analysis of renal tubular cells †," vol. 10, pp. 1–132, 2010, doi: 10.1039/b907515a.

[23] A. Grosberg, A. P. Nesmith, J. A. Goss, M. D. Brigham, M. L. McCain, and K. K. Parker, "Muscle on a chip:

In vitro contractility assays for smooth and striated muscle," *J. Pharmacol. Toxicol. Methods*, vol. 65, no. 3, pp. 126–135, May 2012, doi: 10.1016/j.vascn.2012.04.001.

[24] Y. Imura, Y. Asano, K. Sato, and E. Yoshimura, "A microfluidic system to evaluate intestinal absorption.," *Anal. Sci. Int. J. Japan Soc. Anal. Chem.*, vol. 25, no. 12, pp. 1403–1407, Dec. 2009, doi: 10.2116/analsci.25.1403.

[25] P. M. van Midwoud, M. T. Merema, E. Verpoorte, and G. M. M. Groothuis, "A microfluidic approach for in vitro assessment of interorgan interactions in drug metabolism using intestinal and liver slices," *Lab Chip*, vol. 10, no. 20, pp. 2778–2786, 2010, doi: 10.1039/C0LC00043D.

[26] N. Franzen, W. H. van Harten, V. P. Retèl, P. Loskill, J. van den Eijnden-van Raaij, and M. IJzerman, "Impact of organ-on-a-chip technology on pharmaceutical R&D costs," *Drug Discov. Today*, vol. 24, no. 9, pp. 1720–1724, 2019, doi: 10.1016/j.drudis.2019.06.003.

[27] W. H. van Harten, A. Wind, P. de Paoli, M. Saghatchian, and S. Oberst, "Actual costs of cancer drugs in 15 European countries," *Lancet Oncol.*, vol. 17, no. 1, pp. 18–20, Jan. 2016, doi: 10.1016/S1470-2045(15)00486-6.

[28] E. Alzate, "Medición de temperatura : sensores termoeléctricos," no. June, 2016.

[29] I. Terasaki, "Thermal Conductivity and Thermoelectric Power of Semiconductors," *Ref. Modul. Mater. Sci. Mater. Eng.*, 2016, doi: 10.1016/B978-0-12-803581-8.00771-2.

[30] A. Alashkar and A. H. Alami, "Overview of Thermoelectric Materials," in *Encyclopedia of Smart Materials*, Elsevier, 2022, pp. 319–325.

[31] L. Moreira, "Medição de Temperatura Usando-se Termopar," *Cerâmica Ind.*, vol. 7, no. 5, pp. 51–53, 2002, [Online]. Available: http://www.ceramicaindustrial.org.br/pdf/v07n05/v7n5_6.pdf.

[32] "Overview of Temperature Sensors - NI." https://www.ni.com/pt-pt/innovations/white-papers/06/overview-of-temperature-sensors.html (accessed Oct. 20, 2020).

[33] C. F. Tsai, L. T. Li, C. H. Li, and M. S. Young, "Implementation of thermistor linearization using LabVIEW," *IIH-MSP 2009 - 2009 5th Int. Conf. Intell. Inf. Hiding Multimed. Signal Process.*, vol. 1, pp. 530–533, 2009, doi: 10.1109/IIH-MSP.2009.98.

[34] S. Mokhatab, W. A. Poe, and J. Y. Mak, "Gas Processing Plant Automation," *Handb. Nat. Gas Transm. Process.*, pp. 615–642, 2019, doi: 10.1016/B978-0-12-815817-3.00020-4.

[35] J. Y. Hu, Y. I. Li, and K. W. Yeung, "In vivo physiological measurements," *Cloth. Biosensory Eng.*, pp. 285–300, 2006, doi: 10.1533/9781845691462.285.

[36] V. V. Gureyev and A. A. L'vov, "High accuracy semiautomatic calibration of industrial RTDs," *Conf. Rec. - IEEE Instrum. Meas. Technol. Conf.*, pp. 1–5, 2007, doi: 10.1109/imtc.2007.379291.

[37] V. K. Natrajan and K. T. Christensen, "Temperature Measurement, Methods," in *Encyclopedia of Microfluidics and Nanofluidics*, D. Li, Ed. Boston, MA: Springer US, 2008, pp. 1994–2005.

[38] S. A. Binsilm, M. A. Rad, and M. R. Ahmad, "Modeling of integrated nanoneedle-microfluidic system for single cell temperature measurement," *Appl. Sci.*, vol. 6, no. 12, 2016, doi: 10.3390/app6120339.

[39] J.-M. Yang, H. Yang, and L. Lin, "Quantum Dot Nano Thermometers Reveal Heterogeneous Local Thermogenesis in Living Cells," *ACS Nano*, vol. 5, no. 6, pp. 5067–5071, 2011, doi: 10.1021/nn201142f.

[40] J. Lee, A. O. Govorov, and N. A. Kotov, "Nanoparticle assemblies with molecular springs: A nanoscale thermometer," *Angew. Chemie - Int. Ed.*, vol. 44, no. 45, pp. 7439–7442, 2005, doi: 10.1002/anie.200501264.

[41] C. Espenel, M. C. Giocondi, B. Seantier, P. Dosset, P. E. Milhiet, and C. Le Grimellec, "Temperature-dependent imaging of living cells by AFM," *Ultramicroscopy*, vol. 108, no. 10, pp. 1174–1180, Sep. 2008, doi: 10.1016/j.ultramic.2008.04.090.

[42] C. Li, P. M. Wu, J. Han, and C. H. Ahn, "A flexible polymer tube lab-chip integrated with microsensors for smart microcatheter," *Biomed. Microdevices*, vol. 10, no. 5, pp. 671–679, 2008, doi: 10.1007/s10544-008-9178-3.

[43] N. Inomata, M. Toda, M. Sato, A. Ishijima, and T. Ono, "Pico calorimeter for detection of heat produced in an individual brown fat cell," *Appl. Phys. Lett.*, vol. 100, no. 15, 2012, doi: 10.1063/1.3701720.

[44] P. Schmitt, K. Wedrich, L. Müller, H. Mehner, and M. Hoffmann, "Design, fabrication and characterisation of a microfluidic time-Temperature indicator," *J. Phys. Conf. Ser.*, vol. 922, no. 1, 2017, doi: 10.1088/1742-6596/922/1/012004.

[45] J. Oiler and H. Yu, "Thermoelectric Cool-film Flow Sensor," 2012.

[46] C. Li, J. Sun, Q. Wang, W. Zhang, and N. Gu, "Wireless Thermometry for Real-Time Temperature Recording on Thousand-Cell Level," *IEEE Trans. Biomed. Eng.*, vol. 66, no. 1, pp. 23–29, 2019, doi: 10.1109/TBME.2018.2836949.

[47] J. Qiao, X. Mu, and L. Qi, “Construction of fluorescent polymeric nano-thermometers for intracellular temperature imaging: A review,” *Biosens. Bioelectron.*, vol. 85, pp. 403–413, 2016, doi: https://doi.org/10.1016/j.bios.2016.04.070.

[48] Y. G. Shellman *et al.*, “Fast response temperature measurement and highly reproducible heating methods for 96-well plates,” *Biotechniques*, vol. 36, no. 6, pp. 968–976, 2004, doi: 10.2144/04366ST01.

[49] D. J. King, “Resistance Elements and RTD ’s,” [Online]. Available: http://www.omega.com/temperature/Z/pdf/z054-056.pdf.

[50] A. Komolafe, R. Torah, H. Nunes-Matos, M. Tudor, and S. Beeby, “Integration of temperature sensors in fabrics,” *FLEPS 2019 - IEEE Int. Conf. Flex. Printable Sensors Syst. Proc.*, 2019, doi: 10.1109/FLEPS.2019.8792294.

[51] E. J. P. Santos and I. B. Vasconcelos, “RTD-based smart temperature sensor: process development and circuit design,” *“2008 26th Int. Conf. Microelectron. Proceedings, MIEL 2008,”* no. Miel, pp. 333–336, 2008, doi: 10.1109/ICMEL.2008.4559289.

[52] M. S. Abo Ghazala, H. A. Othman, L. M. Sharaf El-Deen, M. A. Nawwar, and A. E. H. B. Kashyout, “Fabrication of nanocrystalline silicon thin films utilized for optoelectronic devices prepared by thermal vacuum evaporation,” *ACS Omega*, vol. 5, no. 42, pp. 27633–27644, 2020, doi: 10.1021/acsomega.0c04206.

[53] S. Li *et al.*, “Tunable optical properties of amorphous-like ga2o3 thin films deposited by electron-beam evaporation with varying oxygen partial pressures,” *Nanomaterials*, vol. 10, no. 9, pp. 1–10, 2020, doi: 10.3390/nano10091760.

[54] M. El-Dairi and R. J. House, “Optic nerve hypoplasia,” *Handbook of Pediatric Retinal OCT and the Eye-Brain Connection*. pp. 285–287, 2019, doi: 10.1016/B978-0-323-60984-5.00062-7.

[55] H. Tanaka, “Epitaxial Growth of Oxide Films and Nanostructures,” in *Handbook of Crystal Growth: Thin Films and Epitaxy: Second Edition*, vol. 3, Elsevier Inc., 2015, pp. 555–604.

[56] L. Wei, X. Shusheng, and Z. Xiaojun, “Lead-Wire-Resistance Compensation Technique,” *Sensors*, vol. 20,2742, 2020.

[57] T. Junsing, “Interface Circuit for Three-Wire Resistance Temperature Detector with Lead Wire Resistance Compensation,” no. 2, pp. 1–4, 2020, doi: 10.1109/ri2c48728.2019.8999909.

[58] K. Erkan, B. Akkoyunlu, E. Balkan, and M. Tayanç, “A portable borehole temperature logging system using the four-wire resistance method,” *J. Geophys. Eng.*, vol. 14, no. 6, pp. 1413–1419, 2017, doi: 10.1088/1742-2140/aa7ffe.

[59] P. J. Sousa, V. C. Pinto, V. H. Magalhães, R. O. Rodrigues, P. C. Sousa, and G. Minas, “Development of highly sensitive temperature microsensors for localized measurements,” *Appl. Sci.*, vol. 11, no. 9, 2021, doi: 10.3390/app11093864.

[60] Precise, “Thermometer Calibration by the Fixed Point Method - PTS.” http://precisecalibrations.com/thermometer-calibration-fixed-point-method/ (accessed Dec. 30, 2020).

[61] O. Soa, “L79 datasheet,” *STMicroelectronics*, no. January, 2018, [Online]. Available: https://www.st.com/resource/en/datasheet/l79.pdf.

[62] F. P. Dpak, “Positive voltage regulator ICs,” no. February, pp. 1–59, 2016.

[63] S. Lm, “LM134 / LM234 / LM334 3-Terminal Adjustable Current Sources,” no. March 2000, 2013.

[64] D. Information, A. Example, and B. Diagram, “TMUX1108 5V / ± 2 . 5V , Low-Leakage-Current , 8 : 1 Precision Multiplexer,” 2018.

[65] A. Devices, “AD620 Low Cost, Low Power Instrumentation Amplifier,” *Online] www. datasheetcatalog. com.[Online]*, pp. 1–20, 1999, [Online]. Available: http://scholar.google.com/scholar?hl=en&btnG=Search&q=intitle:Low+Cost+Low+Power+Instrumentation+Amplifier+AD620#0%5Cnhttp://scholar.google.com/scholar?hl=en&btnG=Search&q=intitle:Low+Cost,+Low+Power+Instrumentation+Amplifier+AD620#0.

[66] INAx126, “MicroPower Instrumentation Amplifier Single and Dual Versions,” *Texas Instruments*, p. 34, 2015, [Online]. Available: https://tinyurl.com/y228rxyw.